Changes in dissolved organic matter composition and dynamics in a subtropical mangrove river driven by rainfall

Kida, Morimaru ; Tanabe, Mai ; Tomotsune, Mitsutoshi ; Yoshitake, Shinpei ; Kinjo, Kazutoshi ; Ohtsuka, Toshiyuki ; Fujitake, Nobuhide

(Citation)
Estuarine, Coastal and Shelf Science,223:6-17

(Issue Date)
2019-07-31

(Resource Type)
journal article

(Version)
Accepted Manuscript

Changes in dissolved organic matter composition and dynamics in a subtropical mangrove river driven by rainfall

Journal: Estuarine, Coastal and Shelf Science

Morimaru Kida[1†‡*], Mai Tanabe[1], Mitsutoshi Tomotsune[1¶], Shinpei Yoshitake[2¶] Kazutoshi Kinjo[3], Toshiyuki Ohtsuka[4], and Nobuhide Fujitake[1]

1 Graduate School of Agricultural Science, Kobe University, 1 Rokkodai, Nada, Kobe, Hyogo 657-8501, Japan

†Research Fellow of Japan Society for the Promotion of Science

2 Takayama Field Station, River Basin Research Center, Gifu University, 919-47, Iwai, Takayama, Gifu 506-0815, Japan

3 Faculty of Agriculture, University of the Ryukyus, 1 Senbaru, Nishihara, Nakagami, Okinawa 903-0213, Japan

4 River Basin Research Center, Gifu University, 1-1 Yanagito, Gifu, Gifu 501-1193, Japan

‡ Present address: Research Group for Marine Geochemistry (ICBM-MPI Bridging Group), Carl von Ossietzky University of Oldenburg, Institute for Chemistry and Biology of the Marine Environment (ICBM), Carl-von-Ossietzky-Str. 9-11, 26129 Oldenburg, Germany

¶ Present address: Faculty of Education and Integrated Arts and Sciences, Waseda University, 2-2 Wakamatsu, Shinjuku, Tokyo 162–8480, Japan

***Corresponding author**: Morimaru Kida

Institutional address: m.kida@people.kobe-u.ac.jp

Private address: marumori1004@gmail.com

Tell: 078-803-5846

ORCID ID: 0000-0002-9908-2012 (M.K.)

Abstract

Dissolved organic matter (DOM) plays an important role in sustaining ecosystem services of mangrove forests through well-described biogeochemical and ecological functions. This study was conducted in the Fukido River (Ishigaki Island, Japan) to better understand the seasonal and episodic changes in DOM concentration and composition in a subtropical mangrove system. Water samples were collected seasonally along a headwater–mangrove–sea transect on 10 occasions from September 2014 through June 2016. DOM was fractionated based on hydrophobicity into two fractions (hydrophobic and hydrophilic) and also analyzed by excitation-emission matrix spectroscopy combined with parallel factor analysis (PARAFAC). Although seasonal changes in DOM concentration and composition were not observed, both hydrophobic and hydrophilic DOM concentrations and levels of the identified three PARAFAC components clearly increased during a typhoon event. It is suggested that episodic increases in freshwater input due to a typhoon caused enhanced leaching of DOM from mangrove litter and dissolution of mangrove soil organic matter (SOM), which was otherwise retained in the mangrove soil by salinity-induced aggregation. The aggregation–dissolution properties of SOM are crucial in determining the magnitude of DOM outwelling and possibly SOM accumulation rate by enhancing advective DOM exchanges. Future studies are needed to evaluate the size of the carbon pool and outwelling of DOM after classifying mangrove forests based on the hydrological regime that influences biogeochemical conditions in the forests.

Keywords: Aggregation; Blue carbon; DOM; Dissolution; Hydrological regime; SOM

Regional Index Terms: Japan, Okinawa, Ishigaki, Fukido

1 Introduction

Mangrove forests act not only as a large C pool but also as a source of organic matter into the ocean. This is a combined result of their geographical location between land and sea, their large C pool per unit area and organic matter transportation by rivers and tides (Alongi, 2014). Traditionally, it was thought that outwelling of litter from coastal wetlands is a major direct source of energy for the secondary production of estuaries and nearshore waters (Lee, 1995; Odum, 1968). This "outwelling hypothesis" is now considered mostly restricted to the direct vicinity of mangrove forests (Kristensen et al., 2008). One of the primary reasons for this is decomposition of litter to dissolved organic matter (DOM). The litter decomposition takes place with an initial rapid stage (within the first weeks after litter fall) and a later slow stage, and in the initial stage litter can lose up to 60% of its initial weight mainly by DOM leaching (Benner et al., 1990; Wafar et al., 1997). The leached DOM is much more dynamic than litter and will be exported to coastal and even offshore waters, while undergoing photo- and bio-degradation. As a consequence, mangrove DOM can account for as much as 10% of the global transport of terrestrially-derived, refractory DOM to the ocean (based on the global mangrove areal estimate in 2006) (Dittmar et al., 2006).

The role of mangrove forests as a large source of DOM to support the coastal ecosystems is an important topic in mangrove research, and the number of relevant studies has been increasing since 2000 (Cawley et al., 2014; Dittmar et al., 2006, 2001; Maie et al., 2012). A recent study has reported that DOM accounts for >90% of organic matter exported from mangrove forests to the sea (Ray et al., 2018). DOM is a highly heterogeneous collection of organic compounds that collectively play an essential role in key ecosystem processes such as attenuating sunlight and harmful UV radiation (Bricaud et al., 1981), influencing key trace metal speciation (Gledhill and Buck, 2012), and modification of bacterial metabolism (Tranvik, 1992). One of the approaches to fractionate DOM into ecologically meaningful fractions is separation into hydrophobic (HPO) and hydrophilic organic matter (HPI) based on the relative hydrophobicity (Thurman & Malcolm, 1981). HPO, of which main constituents are humic substances (Imai et al., 2001), is the primary metal-binding components in DOM owing to its carboxylic and phenolic functional groups (Blazevic et al., 2016). For example, complexation with iron is essential for oceanic primary productivity; through complexation, HPO can solubilize

74 iron, which would otherwise precipitate and become unavailable for the primary producers in neutral-pH, high-
75 salinity seawater (Gledhill and Buck, 2012). In contrast, HPI, which contains biogenic substances such as
76 proteins, lipids, amino acids, and carbohydrates, is generally biodegradable and can be more easily utilized by
77 heterotrophic bacteria to provide energy and biogenic elements such as C, N, P, and S (Tranvik, 1992). Since
78 HPO and HPI may respond differently to changes in hydrological and biogeochemical conditions and serve
79 different ecological functions, it is essential to examine these DOM fractions independently.

80 Mangrove forests have characteristic physical forces that drive advective groundwater DOM dynamics
81 (Santos et al., 2012). Since groundwater solute concentrations are often higher than overlying waters, these
82 forces can be a source of solutes (DOM, dissolved inorganic carbon, and nutrients) to overlying waters (Santos
83 et al., 2012). Although these forces can exert a major control on the biogeochemistry of sediments and overlying
84 waters, sediment biogeochemistry itself can also affect the magnitude of the advective DOM flux by changing
85 DOM solubility (Kida et al., 2017). The aggregation–dissolution properties of soil organic matter (SOM) due
86 to changes in salinity may be a key mechanism influencing DOM dynamics in mangrove forests. We recently
87 proposed that, in the Fukido mangrove forest, Japan, SOM was accumulated in the soil because of the
88 immobilization of SOM and/or SOM-clay complexes under saline conditions, which serves as one of the
89 mechanisms underlying SOM accumulation in mangrove soils (Kida et al., 2017). This proposition was based
90 on the observation that sequential washing with freshwater (and the corresponding decline in salinity) caused
91 dissolution of SOM from the mangrove soil, but sequential washing with artificial seawater did not. The same
92 phenomenon was also found for soil samples from a Trat mangrove forest, Thailand, irrespective of mangrove
93 species (Kida et al., not published). This finding implies that if sedimentary salinity decreases sufficiently to
94 cause SOM dissolution, for example by an episodic increase in freshwater input due to a typhoon, DOM can be
95 exported by advective exchanges at a higher level than usual. Although this speculation is in line with various
96 literature reporting higher mangrove contribution to DOM in mangrove rivers during rainy seasons and/or
97 episodic rain events (e.g., Cawley et al., 2014), it has not yet been proven in a field study.

98 In this study, we conducted HPO/HPI fractionation along with optical measurements (ultraviolet [UV]-
99 visible absorption spectroscopy and excitation-emission matrix spectroscopy [EEM]) to better understand the

seasonal and episodic changes in DOM concentration and composition along a headwater–mangrove–sea transect in the Fukido mangrove, which was located at the northern limit of mangrove habitats. Particular emphasis was given to elucidating influences of a typhoon event on the surface water DOM dynamics and on the exchange of DOM with the mangrove soil. Optical measurements allow for inexpensive and high sample throughput measurements and require small volumes of water. Optical parameters derived from such measurements have been linked to DOM quality, composition, and biogeochemical processing (Helms et al., 2008; Huguet et al., 2009; McKnight et al., 2001; Spencer et al., 2012; Weishaar et al., 2003) and thus have the potential to improve our understanding of DOM dynamics in complex aquatic environments, like mangrove rivers.

2 Materials and Methods

2.1 Study site and sampling

The study was conducted in the Fukido River, which passes through a mangrove forest on Ishigaki Island, Okinawa, Japan (Fig. 1a). The climate on Ishigaki Island is subtropical, with an annual mean temperature of 24.3°C and annual precipitation of 2,107 mm. Precipitation in May to October is relatively larger than the rest of the year, mainly due to typhoons, accounting for 60% of the annual precipitation, with August and September each having approximately twice as much monthly precipitation as December to March (between 1981 and 2010, Ishigakijima Local Meteorological Observatory [ILMO], Fig. 1b). Broadleaf forests occupy about 95% of the watershed (2.38 km^2, excluding the mangrove forest) with the rest of land use being sparse sugar cane and paddy fields (0.11 km^2), and the river is subject to little human activity. The soil in the catchment is red-yellow soil with a thin A horizon and a low SOM content, which is common in subtropical and tropical areas with high SOM biodegradation rates. The Fukido mangrove forest is a small (0.19 km^2, estimated by Google Earth Pro) mangrove forest vegetated by *Rhizophora mucronata* and *Bruguiera gymnorrhiza* and is registered as a national park. A detailed study of species composition, biomass, and aboveground net primary productivity of this mangrove forest has been reported elsewhere (Ohtsuka et al., 2019). Respiratory mangrove roots protrude from the soil surface and there is no understory and litter layer. The forest soil is mineral rather than peaty (sand

126 contents of 60%–70%) and has a depth of about 1 m before the bedrock. The tentative soil type is gley soil, and
127 a soil organic carbon content does not change systematically with depth and vary between 2% and 5% (Kida et
128 al., not published). There are many notable burrowing macro fauna, such as fiddler crabs (*Uca dussumieri, U.*
129 *vocans,* and *U. tetragonon*), soldier crabs (*Scopimera globose*, *Mictyris brevidactylus)*, and mud shrimps
130 (*Thalassina anomala*). Their burrows could serve as storage points and batch reactors for DOM production
131 (Maher et al., 2013; Stieglitz et al., 2013). The Fukido River is short (<1.5 km) and has an area of 0.015 km^2
132 (7.9% of the mangrove forest) within the mangrove forest. The Fukido River has a clear semidiurnal tide (two
133 tidal cycles per day) within the mangrove forest, with maximum tidal height reaching more than 1 m during
134 spring tide (Ohtsuka et al., 2019). Owing to its small size, the Fukido River is ideal for whole-system water
135 sampling.

136 Surface water samples were collected along a headwater–mangrove–sea transect at seven points as
137 shown in Fig. 1. They were directly collected in 280-mL volume transparent polyethylene terephthalate bottles
138 after rinsing more than three times with the collected water. Preliminary experiments found that DOC
139 contamination from the bottles in the time course of up to nine months was under the detection limit of the total
140 organic carbon analyzer used (<0.05 mgC L^{-1}). A total of 68 samples were collected approximately seasonally
141 on 10 occasions from September 2014 through June 2016 (Table 1, Fig. 2). The pH and salinity (*S,* Practical
142 Salinity Scale) measurements were conducted in situ with portable meters (LAQUAtwin series, HORIBA,
143 Japan). The pH values ranged 7.1–8.3 and generally increased towards downstream areas (Table 1). All
144 sampling was conducted at low tide when outwelling of mangrove-derived materials would be highest (Dittmar
145 et al., 2001), but differed in the extent of rainfall effect (baseflow or not). The baseflow condition was defined
146 as any period more than 24 h after a rain event (7 out of the 10 occasions were under the baseflow condition).
147 On 24–26 August 2015, successive three-day sampling was conducted to capture the changes in DOM
148 concentrations and compositions caused by heavy rain due to a typhoon, named Goni (Category 4 according to
149 the Saffir–Simpson Scale). The typhoon passed through Ishigaki Island at around 20:00 on 23 August 2015.
150 The precipitation on 23, 24, 25 and 26 August was 241, 33, 54 and 14 mm, respectively (ILMO). Samples were
151 kept cooled in the dark during transportation back to the laboratory and filtered within 24 hours of collection

152 with a water- and sample-cleaned glass fiber filter (ADVANTEC GF-75, nominal pore size of 0.3 μm). Carbon
153 contamination from the filter was negligible (<0.01 mg C L^{-1}) according to this protocol. The exception was
154 the series of samples collected during the typhoon event, which was filtered within 1–2 days of collection. The
155 filtered samples were stored in the dark at 4°C and analyzed within one week of collection.
156 Groundwater collection was conducted on 8 March 2016 by a soil water sampler (DIK-8392, Daiki
157 Rika Kogyo, Saitama, Japan) every 2 h for 24 h, thus covering two tidal cycles. Five 1-m vinyl chloride pipes
158 with a porous ceramic cup (18 × 60 mm) attached at the head were inserted to a depth of 20, 40, 60, 80, and
159 100 cm with care not to disturb soil, and groundwater (50 mL each) was collected by syringe. It took about 30
160 min per sampling to fill the syringe with groundwater. We also attempted to collect groundwater during the
161 typhoon event at a place closer to the sea than on 8 March 2016 (Fig. 1). However, because of the difficulties
162 of monitoring during the massive typhoon, we could only collect groundwater samples a few days after the
163 typhoon (26–27 August 2015). The sampling settings were almost identical to the 8 March 2016 groundwater
164 sampling (i.e., 20, 40, 60, and 80 cm depth every 2 h for 30 h). The groundwater samples were transported,
165 prepared, and analyzed the same way as surface water samples.
166
167 **2.2 DOM fractionation**
168 The water samples were fractionated into HPO and HPI as described by Tsuda et al. (2012). The validity of the
169 method for samples with different salinities was previously confirmed (Kida et al., 2016). Briefly, 0.4 mL of
170 purified DAX-8 resin (ground to 50–200 μm) was weighed into a glass vial with a Teflon screw cap, and 20
171 mL of the sample was added and acidified with 1 mL 1M H_2SO_4 (special grade, Wako, Japan) to adjust the pH
172 to <2. After shaking for 24 h, the dissolved organic carbon (DOC) concentration of the supernatant, the HPI
173 fraction, was analyzed after filtration through a GF-75 glass fiber filter. The HPO concentrations were
174 calculated as the difference between the bulk DOC concentration and the HPI concentration. Organic C
175 contamination from the system was determined with ultrapure water as a blank and used for correction (<0.1
176 mg C L^{-1}). Both the blank determination and HPO adsorption were conducted in triplicate or quadruplicate,
177 consuming <100 mL of each sample. The precision of the replicate measurements was 2.8% for the average

coefficient of variation (CV) of all the measurements, and the average values were used for data analysis and are reported here. Although the DOM fractions retained on the DAX-8 resin can also include hydrophobic neutrals, their contribution to DOM is generally very small in natural rivers (Imai et al., 2001), and thus we assumed that the HPO fraction was almost exclusively occupied by humic substances. All glassware was acid-washed and muffled at 450°C for more than 3 h before use to minimize possible contamination.

The DOC was measured as non-purgeable organic carbon in a total organic carbon analyzer (TOC-L_{CPH}, Shimadzu, Japan) by the platinum-catalyzed high-temperature combustion method coupled to non-dispersive infrared gas detection of CO_2. Each sample was first sparged with a carrier gas for 90 s in the built-in syringe of the TOC analyzer after acidification to remove any inorganic C prior to combustion. Calibration was performed by running four standards of a potassium hydrogen phthalate solution over an appropriate range and one laboratory blank (ultrapure water). The elemental concentrations were calculated from the regression line (coefficient of determination, $R^2 > 0.999$). Reported DOC concentrations are average values of triplicate measurements. Samples were analyzed with repeated injections with the criteria that the peak area CV was <2.0% or the SD was <0.2, whichever was lower. If the CV or SD exceeded the thresholds, up to two additional analyses were performed and the most deviated outliers were eliminated.

2.3 Optical measurements

UV-visible absorption spectra (240–600 nm) were measured using a UV-visible spectrophotometer (V-630, JASCO, Japan) with a 5-cm path length, acid-cleaned, quartz cuvette at ambient temperature. Measurements were baseline-corrected using ultrapure water. The $SUVA_{254}$ was calculated by dividing the UV absorbance (m^{-1}) measured at $\lambda = 254$ nm by the DOC concentration (mg C L^{-1}) and reported in L mg C^{-1} m^{-1}. The $SUVA_{254}$ was originally reported by Weishaar et al. (2003) to be correlated with percent aromaticity of isolated humic substances and later used as a surrogate for DOM aromaticity in a number of studies. Although the presence of Fe has been shown to influence $SUVA_{254}$ (Weishaar et al., 2003), a preliminary measurement with inductively coupled plasma atomic emission spectrometry found that Fe concentrations in the Fukido River were low (under

the detection limit of the analyzer, 10 $\mu g L^{-1}$), and correction for Fe was not carried out. Napierian absorption coefficients, $a(\lambda)$, of DOM were calculated as follows:

$a(\lambda) = 2.303A(\lambda)/l$

where $A(\lambda)$ is the measured absorbance at wavelength λ and l is the cell path length in meters (Hu et al., 2002). Spectral slope ($S_{275–295}$), which has been related to apparent molecular weight and degree of photochemical and microbial processing and used as a source differentiation (terrestrial vs marine) tool in estuarine studies (Fichot and Benner, 2012; Helms et al., 2008), was calculated using a linear fit to the natural log-transformed $a(\lambda)$ spectrum in the ranges of 275–295 nm. Typically, a higher (steeper) $S_{275–295}$ value suggests a decrease in molecular weight and aromaticity of DOM and an increase in the degree of photodegradation.

Fluorescence EEMs were collected with a spectrofluorometer (FP-6200, JASCO, Japan) equipped with a 150 W xenon arc lamp at room temperature using 5 nm excitation and emission slit widths, a scan speed of 500 nm min^{-1}, an excitation (Ex) range of 240–450 nm at 5 nm increments, and an emission (Em) range of 300–550 nm at 1 nm increments. The EEMs were measured for the samples collected after August 2015 (n = 42). Fluorescence signals were acquired in signal-to-reference mode to eliminate intensity fluctuations of the xenon lamp. Excitation wavelengths below 265 nm were removed due to deteriorating signal-to-noise ratios. Because inner filter effects (IFE) produce a suppression of 5% or more against true fluorescence intensity when absorbance exceeds 0.042 (Kothawala et al., 2013), primary and secondary IFE corrections were applied to each sample EEM using the absorbance of the corresponding sample in a 1-cm path length quartz cuvette (Kothawala et al., 2013). The absorbance of all of the samples across the full EEM was less than 0.17. Subsequently, an ultrapure water EEM measured on the same day as the samples was subtracted from each of the IFE-corrected EEMs. Fluorescence intensities were normalized in Raman units (RU) using the Raman peak measured at an excitation of 350 nm obtained from the ultrapure water EEM. We note that in Raman normalization, the Raman peak was baseline corrected at an emission range of 371–428 nm, and only the Raman peak area was used (corresponding to emission range of approximately 388–410 nm), as in Murphy (2011).

The biological index (BIX) was obtained from the corrected and Raman-normalized EEMs. The BIX is calculated as the ratio of emission intensities at 380 nm and 430 nm (I380/I430) at an excitation of 310 nm

and estimates autochthonous biological activity in water environments (Huguet et al., 2009). High values (>1) of BIX correspond to DOM of predominantly autochthonous origin and to freshly released DOM in water, whereas lower values (0.6–0.7) correspond to low DOM production in natural waters (Huguet et al., 2009). Although corrections for the effect of the instrument-specific response on EEMs were not applied because of the lack of a manufacturer-provided correction factor, the trend for BIX values on DOM source interpretation is robust (Huguet et al., 2009).

2.4 PARAFAC analysis

We analyzed the EEMs by parallel factor analysis (PARAFAC) to mathematically deconvolute them into distinct fluorescent components with independent spectral characteristics. We used Matlab R2017b with the *drEEM* toolbox (v 0.4.0) (Murphy et al., 2013). A sample set (n = 6), which was collected on 1 June 2015 when precipitation of 17 mm was recorded, was included in the PARAFAC analysis (total of 48 samples). EEMs were normalized to total fluorescence intensities to account for the differences in fluorescence intensity among samples and reduce correlations between PARAFAC components. During the exploratory phase, eight outliers were removed based on their leverage. The model was constrained to non-negative values. Models (3–5 components) were developed with a convergence criterion of 10^{-8}. Each model was iterated 10 times after initializing with random starting values, and only the least squares solution was retained. The final three-component model accounted for >98.8% of the measured spectral variation and had a core consistency value of 53.4%. The appropriate component number was determined by residual analysis and split-half analysis (S4C6T3; Murphy et al., 2013). The identified components were quantitatively compared with the published data using an open-access spectral database (OpenFluor; Murphy et al., 2014). On OpenFluor, one can compare fluorescence datasets and determine Tucker congruence coefficient (TCC) between pairs of excitation (TCC_{ex}) and emission (TCC_{em}) spectra. If an identified fluorescent component has a strong match ($TCC_{ex \times em} > 0.95$), it means that the same or a spectrally indistinguishable validated component had been reported in the literature. After the model building, the outliers were projected onto the validated model to obtain scores for them. However, three out of the eight samples were not adequately modeled (judged by residuals), and thus their

PARAFAC results are not presented. The fluorescence intensity at the maximum for each component was represented by F_{max} (in RU) (Murphy et al., 2014). Although the EEMs in this study were not corrected for the instrument-specific bias, the PARAFAC results can be internally compared because they were obtained with the same instrument under identical conditions.

2.5 Data analysis

The percent contribution of DOM, HPO, HPI, and PARAFAC components from the mangrove forest were estimated according to Cawley et al. (2014). Briefly, the difference between the area under the conservative mixing line and the area under the measured data was divided by the area under the measured data and multiplied by 100 to get the percentage values. The data points were interpolated by 0.1 salinity increments. The conservative mixing line was determined by fitting a line between the headwater and sea samples on each day. On 10 November 2015 and 8 March 2016, the seawater sample collected on 20 June 2016 was used as a seawater endmember for PARAFAC components because the PARAFAC model was not well fitted to the seawater samples on these days. On 20 June 2016, the sample collected at the upper end of the mangrove forest was used as a river endmember because it had a lower DOC concentration than the headwater sample while having almost same salinity. In addition, on 25 and 26 August 2015, the seawater sample collected on 24 August 2015 was used as a seawater endmember because we could not collect a seawater endmember on these days because of dilution of seawater by intense rainfall (Table 1, Fig. 3). Our seawater endmembers were not a pure seawater end member because of relatively low salinity ($S < 32$), and thus this method likely conservatively estimates the mangrove contribution, assuming that seawater had lower DOM concentration and fluorescence intensity. A two tailed F-test (95% confidence level) was used to determine whether measurements were statistically different from the conservative mixing line.

Statistical analysis was carried out using Origin 2016 (OriginLab Corporation, MA, USA). Differences between DOC concentrations, the proportions of HPO in DOM (%HPO), or values of optical indices under the baseflow conditions and during the typhoon event were analyzed by the Student's t-test. The statistical difference between multiple parameters was tested by Tukey-Kramer's multiple comparisons of means when

the normality and homogeneity of variance was confirmed by Shapiro-Wilk test and Leven's test, respectively. A significance level of 0.05 was selected for the t-test and Tukey-Kramer's multiple comparisons to test the null hypothesis. Correlations between parameters were analyzed by linear regression analysis. Linear correlations were considered statistically significant when $P < 0.01$.

3 Results

3.1 DOM distribution along the salinity gradient

In the first year, we collected water samples seasonally from September 2014 (summer) to May 2015 (spring) (Table 1). The intention was to capture the seasonal changes in DOC concentrations and DOM compositions (i.e., %HPO). However, we did not observe significant seasonal changes (Tukey-Kramer, $P > 0.05$). A preliminary sampling on a heavy rainy day in May 2013 showed higher DOC concentrations and %HPO than under the baseflow conditions (Table S1). Therefore, in the second year, water sampling during a heavy storm event was planned. The expectation was that the changes in concentrations and compositions of DOM would be observed, allowing us to assess whether an episodic heavy rain event affects DOM dynamics. We successfully collected samples during a typhoon event on 24–26 August 2015 (Typhoon Goni, Fig. 2).

The DOM fractionation results are given in Fig. 3 with the HPO and HPI concentrations as well as DOM concentrations plotted against salinity (only data with PARAFAC results are shown for clarity; see Fig. S1 for other results). The DOM concentrations ranged between 0.67 and 3.71 mg C L^{-1}, while the HPO and HPI concentrations ranged from 0.29 to 2.34 mg C L^{-1} and 0.22 to 1.37 mg C L^{-1}, respectively. Both HPO and HPI showed positive deviations from conservative mixing, indicating that there were inputs of both HPO and HPI from the mangrove forest, although the non-conservative behavior of HPI was less pronounced than HPO. An exception was observed on 20 June 2016, when the headwater sample had a higher HPO and HPI concentration than a sample collected at the upper end of the mangrove forest. Nevertheless, under the baseflow conditions, on average 25% ± 13%, 22% ± 12%, and 15% ± 17% of DOM, HPO, and HPI were contributed from the mangrove forest to the Fukido River, respectively (Fig. 3, Table 3). On 24–26 August 2015, when the catchment had heavy rain due to Typhoon Goni, the DOC concentrations increased, especially at the headwater

307 and the second sampling point, compared with values under the baseflow conditions (2.48 ± 0.90 vs 1.20 ± 0.35
308 mg C L^{-1}, Table 1, $P < 0.001$), suggesting a supply of organic materials from the catchment and mangrove
309 forest. During the typhoon event, the DOC concentrations increased day by day for all sampling points except
310 for at the headwater. The sharp DOC increases at the sampling point located at the upper end of the mangrove
311 forest were most notable (Fig. 3, Table 1). Moreover, salinity decreased day by day despite the identical
312 sampling positions and timing (i.e., all at low tide), indicating that seawater was diluted by freshwater because
313 of the heavy rain, at least until the estuarine sampling point. During the typhoon event, 24% ± 3% and 29% ±
314 3% of DOM and HPI were contributed from the mangrove forest to the Fukido River, respectively (Fig. 3,
315 Table 3). The contribution of the mangrove forest to HPO was on the same order as to DOM and HPI, but it
316 was insignificant during the typhoon event ($P > 0.05$).
317 The proportions of HPO in DOM (%HPO), based on C concentrations, showed a similar trend along
318 the salinity gradient irrespective of sampling days (Fig. 4). The %HPO ranges were 33.6%–71.0% and
319 decreased with the increase in salinity. The highest and lowest %HPO were observed at the headwater and the
320 sea, respectively. The mean %HPO (±SD) at the headwater and the sea was 68.2% ± 2.1% and 46.7% ± 7.4%,
321 respectively. The mean %HPO at the headwater under the typhoon and baseflow conditions was 69.6% ± 1.1%
322 and 67.1% ± 1.5% and slightly higher during the typhoon event, although the difference was not significant (P
323 = 0.055).
324 Figure 5 shows groundwater DOC concentrations at different depths. The DOC concentrations of the
325 groundwater increased with depth and were ~3 times higher than the surface water DOC concentration
326 measured at the closest point during the low tide on the same day (1.18 mg C L^{-1}, Table 1). Although just a
327 snapshot, this implies that groundwater would necessarily be a source of DOC to the surface water of the Fukido
328 River if advective groundwater exchanges occurred.
329
330 **3.2 Optical parameters**
331 The distribution patterns of the measured optical parameters as well as %HPO are plotted against salinity in
332 Fig. 4. The $SUVA_{254}$ decreased with the increase in salinity as in %HPO, showing high values at the headwater

(3.1–4.2 L mg C^{-1} m^{-1}) and low values at the sea (0.8–3.0 L mg C^{-1} m^{-1}). The BIX values fluctuated between 0.55 and 0.76 until S = 15–20, then rapidly increased up to 0.93 at the sea sampling point. The $S_{275–295}$ varies between 0.011 and 0.019 nm^{-1} and consistently increased along with salinity except for in November 2016 when seawater samples irregularly had a lower value than the corresponding estuarine sample. When comparing values of the optical indices within the mangrove forest ($0.05 < S < 15$) under the baseflow and typhoon conditions, $SUVA_{254}$ values were significantly lower (3.3 ± 0.3 versus 3.7 ± 0.3) and BIX values were higher (0.67 ± 0.04 versus 0.61 ± 0.04) during the typhoon event than under the baseflow conditions ($P < 0.05$), which was against our expectation. This could be partly explained by inputs of non-humic materials from the mangrove forest canopy, which will be discussed later. At the same salinity range, the difference in %HPO during the typhoon event and under the baseflow conditions was not significant ($P = 0.75$).

3.3 PARAFAC components

Three components were identified by PARAFAC analysis of the Fukido River samples (Fig. S2, Table 2). All of the three components had fluorescence maxima at Em > 350 nm. The components were named according to their rounded fluorescence emission maximum: C_{480}, C_{410}, and C_{380}. C_{480} was composed of two peaks with Ex < 265 nm and 360 nm at Em 478 nm. The fluorescence of C_{410} was blue-shifted relative to C_{480} and had fluorescence peaks at Em 409 nm with Ex < 265 nm and 325 nm. C_{380} had broad fluorescence peaks at approximately Em 310–440 nm (highest at 380 nm) with Ex < 265 nm and 275 nm. The spectral shape of C_{380} was not good, with the emission spectra extending to 550 nm, probably because of the low sample fluorescence intensity and low signal-to-noise ratios of the spectrofluorometer in the UV-C region. Although the EEMs in this study were not corrected for the instrument-specific bias, C_{480} and C_{410} had multiple strong matches ($TCC_{ex×em} > 0.95$) on OpenFluor (36 components for C_{480} and 14 components for C_{410}). Assignments of the components are summarized in Table 2 with descriptions of each component provided in the literature. C_{480} has been found in a wide range of environments and suggested as a ubiquitous, terrestrial humic-like component with high aromaticity (Osburn et al., 2016; Yamashita et al., 2010). C_{410} has also been reported as a ubiquitous humic-like component and suggested as both photo-labile and bio-available (Cawley et al., 2012; Stedmon and

Markager, 2005a; Yamashita et al., 2010). C_{380} had only three matching components with $TCC_{ex \times em} > 0.9$, and they were reported as either a tryptophan-like component (Soto Cárdenas et al., 2017) or combination of several components (including protein-like components) having similar excitation spectra with different emission spectra (Murphy et al., 2018). Considering spectral characteristics and peak positions of C_{380}, this component could be categorized as a combination of a protein-like component and UV-C humic component. We note that the number of the identified PARAFAC components in this study may have been underspecified because of the small sample size (n = 40) (Murphy et al., 2013, 2011; Stedmon and Markager, 2005a). Therefore, C_{380} may be separated into a protein-like component and UV-C humic-like component if the sample size was increased. These components are frequently reported to co-exist in the estuarine environment and river-influenced ocean margins (Cawley et al., 2014; Maie et al., 2014; Yamashita et al., 2015, 2010), which could explain why the PARAFAC analysis could not resolve these components.

The F_{max} of the two humic-like PARAFAC components (C_{480} and C_{410}) had a significant strong correlation with DOC concentrations (both $R^2 = 0.87$, $P < 0.001$). Consequently, they showed very similar non-conservative distributions as DOC concentration irrespective of sampling days, with high values (up to 0.47 RU under the baseflow conditions) within the mangrove forest, and strong decreases with salinity to values ≤0.04 RU at the sea sampling point (Fig. 3). The positive deviations from conservative mixing suggest that there were inputs of these humic-like components from the mangrove forest. C_{380}, in contrast, had a weaker overall correlation with DOC concentrations ($R^2 = 0.79$, $P < 0.001$), and the relationship was particularly weak under the baseflow conditions ($R^2 = 0.33$, $P < 0.01$). Consequently, under the baseflow conditions, C_{380} remained at relatively constant values (mostly < 0.1 RU) along the headwater-mangrove-sea transect, and the distribution patterns of C_{380} were not significantly different from the conservative mixing line in two out of three cases (Table 3). Under the baseflow conditions, on average 42% ± 4%, 46% ± 4%, and 7% ± 10% of C_{480}, C_{410}, and C_{380} were contributed from the mangrove forest to the Fukido River, respectively (Fig. 3, Table 3). In contrast, during the typhoon event, the highest F_{max} value of all the components along the salinity gradient approximately doubled, and the sampling point where the highest F_{max} was observed shifted from at the middle of the mangrove forest to the upper end of the forest (Fig. 3, Table 1), which was consistent with the distribution

385 of the DOM concentrations. During the typhoon event, 37% ± 6%, 42% ± 6%, and 44% ± 11% of C_{480}, C_{410},
386 and C_{380} were contributed from the mangrove forest to the Fukido River, respectively (Fig. 3, Table 3). The
387 contribution of the mangrove forest to C_{380} was significantly higher during the typhoon event than under the
388 baseflow conditions ($P < 0.05$).

389 Relative abundances of each PARAFAC component for each sample EEM ($\%F_{max}$) were calculated to
390 investigate changes in its overall importance (Fig. 3). Under the baseflow conditions, $\%C_{480}$ and $\%C_{410}$ slightly
391 increased while $\%C_{380}$ decreased until S = ~10, reflecting inputs of C_{480} and C_{410} within the mangrove forest.
392 In contrast, at higher salinity regions, $\%C_{480}$ and $\%C_{410}$ monotonically decreased while $\%C_{380}$ increased with
393 salinity, suggesting the dominance of C_{380} in seawater. These results clearly show that general compositions of
394 fluorescent DOM changed along the salinity gradient. Changes in the relative abundance of the components
395 with salinity during the typhoon event were somewhat more variable than under the baseflow conditions, though
396 a similar increasing pattern in $\%C_{380}$ was observed with increasing salinity.
397
398 **4 Discussion**
399 **4.1 DOM composition and distribution in the Fukido River**
400 The behavior of riverine DOM during estuarine mixing has mainly been studied in the context of changes in
401 DOC concentration along salinity gradients. The dynamics of DOM in wetland-influenced coastal rivers can be
402 more complex than the simple mixing of riverine DOM with seawater because of additional DOM supply from
403 wetlands (Cawley et al., 2014; Dittmar et al., 2006; Maie et al., 2012). If we assumed a simple two-endmember
404 mixing model for the DOM fractions and PARAFAC components, all data should be on a straight line
405 (conservative mixing line) connecting headwater and seawater data points. However, the positive deviations of
406 the quantitative parameters along the salinity gradient in Figure 3 indicate significant non-conservative mixing
407 in most cases (Table 3). Although seagrasses and aquatic macrophytes and macroalgae have been suggested as
408 a source of DOM to mangrove rivers (Maie et al., 2012, 2006, 2005), they were not observed within the Fukido
409 mangrove forest, suggesting that the mangroves were the major additional source of DOM to the Fukido River.
410 The increase in the HPO concentrations at S = 5–15 under the baseflow conditions indicates that precipitation

411 (or flocculation) of HPO in the river water was very small and/or the HPO inputs from the mangrove forest
412 were larger than the removal of the riverine HPO, although it is known that humic acids precipitate under the
413 interaction with cations in the seawater even at low salinity range (Sholkovitz, 1976). The HPO inputs from the
414 mangrove forest support the inputs of colored DOM from mangrove forests (Cawley et al., 2014; Dittmar et al.,
415 2006; Maie et al., 2012). We presumed that the HPO supplied from the mangrove forest was dominantly
416 composed of fulvic acids. For example, Fox (1983) reported that, in seven coastal plain estuaries located in the
417 mid-Atlantic US, humic acids were 100% removed during estuarine mixing. In contrast, fulvic acids hardly
418 precipitate (<10%) even in the seawater (Kida et al., 2016). In any case, the supplies of both HPO and HPI with
419 different biogeochemical and ecological roles from the mangrove forest support its importance as a
420 heterogeneous DOM source (Cawley et al., 2014; Dittmar et al., 2006, 2001; Maie et al., 2012). The HPO/HPI
421 fractionation reported here was quantitative, i.e., 100% of DOM was tracked in terms of carbon, in contrast to
422 colored or fluorescent DOM, which represents only a fraction of the total DOC pool. Future studies are
423 encouraged to link DOM composition and primary productivity and/or heterotrophic activity to separately
424 assess the impact of HPO and HPI on coastal ecosystems.

425 %HPO and $SUVA_{254}$ decreased, while BIX and $S_{275–295}$ increased along the headwater–mangrove–sea
426 transect (Fig. 4). These changes are highly likely to represent the general trend in the Fukido River, since they
427 were observed irrespective of sampling day (baseflow/rainy) even when the DOM concentrations and
428 compositions varied. These changes along the salinity gradient indicate the shift in DOM origin from
429 soil/terrestrial (allochthonous) to aquatic production (autochthonous) or photodegraded allochthonous DOM
430 (Helms et al., 2014, 2013). Although similar changes in $SUVA_{254}$ and BIX are often observed in estuaries
431 (Huguet et al., 2009), past literature did not conduct HPO/HPI fractionation. Therefore, the current study is the
432 first, to our knowledge, to elucidate the changes in DOM optical properties in the mangrove settings based on
433 the changes in %HPO. Until approximately $S = 25$, %HPO was >50%, $SUVA_{254}$ was >3 L mg C^{-1} m^{-1}, $S_{275–295}$
434 was <0.016 nm^{-1}, and BIX was <0.7, indicating that the dominant origins of DOM were terrestrial/mangrove
435 SOM. As reported in other studies (Butman et al., 2012; Hanley et al., 2013; Spencer et al., 2012), all of the
436 indices ($SUVA_{254}$, BIX, and $S_{275–295}$) had a significant ($P < 0.001$) moderate correlation with %HPO (Fig. S3).

437 Since the relationships between DOM composition and optical index values can vary from site to site (Hanley
438 et al., 2013), establishing their relationships in a given site of interest is required. As current mangrove river
439 studies are mostly conducted in mangrove forests with peaty soils (Cawley et al., 2014; Dittmar et al., 2006,
440 2001; Maie et al., 2012), the results in this study can serve as a basis for the relationships between the DOM
441 composition and studied optical indices in rivers that flow on mineral mangrove soils in the subtropical climate.
442 The unexplained variation of %HPO values by the optical indices in Fig. S3 indicate the limited potential of
443 these indices to predict %HPO values in this mangrove area, which may be due to the small number of samples
444 and the complex nature of the mangrove biogeochemistry.

445 The PARAFAC analysis of fluorescence EEMs provided further evidence that the mangrove forest
446 functioned as a major contributor of heterogeneous DOM to the Fukido River (Fig. 3, Table 3). The most
447 dominant fluorescence component in the Fukido River was C_{480}, which was reported to ubiquitously exist in a
448 range of environments, including mangrove rivers and salt marshes (Maie et al., 2014; Osburn et al., 2016;
449 Yamashita et al., 2010). A similar PARAFAC component was reported as a dominant component in humic and
450 fulvic acid fractions in estuarine soils and sediments (Santín et al., 2009). Other than humic substances derived
451 from the mangrove soil, mangrove leaf-derived lignin and tannins that underwent oxidative decompositions and
452 polycondensation reactions could be a major source of C_{480} (Maie et al., 2008, 2007). A recent study found a
453 strong relationship between F_{max} values of C_{480} and lignin concentrations and proposed C_{480} as a terrestrial DOM
454 marker (Osburn et al., 2016). The other humic-like component C_{410} has been recognized as ubiquitous in the
455 environment and also reported to be dominant in humic fractions in estuarine soils and sediments (Santín et al.,
456 2009). In the Fukido River, the F_{max} values of C_{480} and C_{410} correlated very well ($R^2 = 0.99$, $P < 0.001$), strongly
457 suggesting that they were derived from the same source and controlled by common environmental processes.
458 Considering that C_{480} and C_{410} existed at high levels both at the headwater and within the mangrove forest, but
459 at low levels in the seawater, they were most likely derived from the catchment and mangrove soil.
460 Photodegradation is a well-known process that decreases red-shifted humic-like fluorescence (Helms et al.,
461 2013). Thus, the low levels of C_{480} and C_{410} fluorescence in seawater samples could result from extensive

462 photodegradation of the terrestrially- and mangrove-derived humic-like fluorescence components, as well as
463 the source difference.

464 In contrast to C_{480} and C_{410}, no systematic changes in Fmax values of C_{380} were observed along the
465 salinity gradient under the baseflow conditions (Fig. 3, Table 3). The fluorescence property of C_{380} could be a
466 combination of protein-like fluorescence and UV-C humic fluorescence. Fluorescence components responsible
467 for these fluorescence were considered photo-refractory because of the blue-shifted excitation maximum
468 (Murphy et al., 2018; Stedmon and Markager, 2005b). The rapid attenuation of UV-B light in the water column
469 would restrict the photodegradation of these components to a thin layer at the surface (Stedmon and Markager,
470 2005b), even though UV-C humic-like fluorescence is intrinsically susceptible to photodegradation (Boehme
471 and Coble, 2000). Thus, it is not surprising that C_{380} was observed at higher relative abundance at the seawater
472 sampling point. Other than proteins, tannins derived from mangrove litter are known to fluoresce in the protein
473 fluorescence region (Maie et al., 2008, 2007). Therefore, there were three possible origins of C_{380} in this study,
474 which were humic substances exported from the catchment and mangrove soil, tannins leached from mangrove
475 litter, and autochthonous production of proteinaceous materials (Stedmon and Markager, 2005b). Because there
476 was no significant import of C_{380} from the mangrove forest under the baseflow conditions (Table 3), it was
477 suggested that C_{380} was likely composed of soil humic substances and proteinaceous materials under the
478 baseflow conditions, with an increasing proportion of proteinaceous materials with increasing salinity (Cawley
479 et al., 2014; Maie et al., 2014; Yamashita et al., 2015, 2010). During the typhoon event, inputs of UV-C humic-
480 like substances from the mangrove soil by dissolution of SOM may have occurred (Kida et al., 2017), because
481 the significant import of C_{380} from the mangrove forest was observed (Fig. 3, Table 3).

482 It is also possible that the contribution from tannins increased during the typhoon event. It has been
483 reported that the mangrove-derived DOM inputs to the surface water increased during a rain event via stemflow
484 and throughfall from the mangrove forest canopy (Twilley, 1985). In addition, we found an exceptionally large
485 amount of litter on the forest floor and river bed after the typhoon, a part of which was quantitatively measured
486 using litter traps (Fig. 8 of Ohtsuka et al., 2019). Leaching of DOM (tannins and possibly other components)

487 from the mangrove litter and canopy could partly explain the increase in C_{380} levels and the shifts in optical
488 index values (Fig. 4) during the typhoon event.
489
490 **4.2 Changes in DOM composition and dynamics in the Fukido River by rainfall**
491 A sharp, spike-like increase in the DOM concentration and the PARAFAC component levels was observed at
492 the sampling point at the upper end of the mangrove forest during the typhoon event (Fig. 3). Several
493 possibilities could be considered as a cause of this, such as elevated DOM supplies by surface water runoff and
494 dissolution of SOM because of the decline in salinity due to the heavy rain followed by advective groundwater
495 exchanges. The first possibility was considered unlikely or little, if any, since during the typhoon event, the
496 distribution patterns of DOM along the salinity gradient was not conservative (Fig. 3) and the increase in DOC
497 concentrations was more pronounced within the mangrove forest than at the headwater (Table 1), indicating
498 additional DOM inputs from the mangrove soil (including groundwater) were primarily responsible for the
499 increase in DOC concentrations and change in composition within the mangrove forest. We note that, even
500 though we did not observe a large increase in DOC concentrations at the headwater, this did not necessarily
501 mean that DOC flux supplied from the catchment remained unchanged. In addition, it is likely that we missed
502 an initial pulsing of heavy rain that often is the most important for DOM export from the terrestrial landscape
503 (Spencer et al., 2008). On the first day of the typhoon event (23 August 2015), a precipitation event of 241 mm
504 was observed, which was considerably higher than that after the typhoon passed (14–54 mm on 24–26 August
505 2015). High surface water runoff and leaching of surface litter and soil layers in the catchment during the initial
506 pulsing of the heavy rain could export a large amount of DOM to the Fukido River (Spencer et al., 2008). Indeed,
507 we observed flooded tributaries that were turbid due to the heavy rain, which were distinctly different under the
508 baseflow conditions. However, since we did not collect water discharge data, we discuss the cause of the
509 increase in the DOC concentration and the PARAFAC component levels during the typhoon event.
510 Another possibility is that dissolution of SOM occurred because of the decline in salinity due to the
511 heavy rain and more DOC was eventually supplied to the Fukido River by advective groundwater exchanges.
512 Among the advective DOM dynamics in mangrove forests described elsewhere (Santos et al., 2012), terrestrial

513 hydraulic gradients, tidal pumping, and mangrove pumping were considered to be mainly responsible for the
514 advective groundwater exchanges during the storm event. This second possibility (advective exchanges of
515 increased-DOC groundwater resulting from dissolution of SOM) has been recently suggested by our laboratory
516 model experiment using the Fukido mangrove soil (Kida et al., 2017). We demonstrated that sequential washing
517 with freshwater (and the corresponding decline in salinity) caused dissolution of SOM from the mangrove soil,
518 but sequential washing with artificial seawater did not. This implies that if sedimentary salinity decreases
519 sufficiently to cause SOM dissolution, DOM can be exported by the advective exchanges at a higher level than
520 usual. The observation in the current study may indicate that SOM accumulated by salinity-induced aggregation
521 was re-mobilized by the increased freshwater input. Such an episodic mobilization of SOM may be limited to
522 where the relative contribution of freshwater is high, such as the upper end of the mangrove forest and the river
523 bed and bank. To investigate whether the decline in salinity due to the storm event occurred where there was a
524 less freshwater influence, we monitored groundwater salinity just after the typhoon event at a place closer to
525 the sea than on 8 March 2016 (Fig. 1). Figure S4b shows that groundwater salinity was considerably lower at
526 first and then gradually increased to reach stable ranges that were similar to, but still lower than, those measured
527 on 8 March 2016 under the baseflow condition (mean S = 28.1, Fig. S4a). This suggests that groundwater
528 salinity decreased by the typhoon and still maintained low values a few days after the typhoon passed. During
529 the typhoon event, the groundwater salinity could have been even lower. Comparing a depth trend in salinity in
530 Figs. S4a and S4b, we noticed that deeper layers tended to have lower salinity after the typhoon event, which
531 was contrary to the depth trend under the baseflow condition (the deeper, the higher salinity). This suggested
532 that groundwater salinity up to ~1 m depth decreased during the typhoon event, further strengthening our
533 hypothesis that the typhoon event decreased groundwater salinity. This decrease in salinity could be a driver of
534 SOM dissolution and supply higher concentrations of DOM to the Fukido River. Thus, the aggregation–
535 dissolution properties of SOM due to changes in salinity may be a key mechanism that influences DOM
536 dynamics in mangrove forests, by enhancing advective DOM exchanges. It is currently unknown if DOM
537 exported via SOM dissolution can be transported over long distances or undergoes re-aggregation upon
538 encountering seawater. However, frequently reported increases in both DOM and turbidity during the rainy

539 season and rainfall events (Dittmar and Lara, 2001; Ray et al., 2018; Twilley, 1985) may indicate that a part of
540 DOM transforms into the particulate phase, although the increase in turbidity is often interpreted as a result of
541 the increase in particulate materials from the catchment and mangrove soils.
542
543 **4.3 Implications for organic matter dynamics of mangrove forest**
544 The controls on DOM dynamics by aggregation–dissolution properties discussed here are relevant to research
545 areas other than mangrove forests such as (i) widespread browning of the surface waters across northern
546 countries and (ii) reduction of DOM export from coastal freshwater wetlands due to saltwater incursion. (i)
547 Increases in DOM concentrations have been observed in freshwater across large areas of Europe and North
548 America. Among several mechanisms that explain the increase, decline in acidity and ionic strength of soil
549 solutions due to a decline in anthropogenic sulfur and sea salt deposition have been proposed as a chemical
550 mechanism (Evans et al., 2006). Increased pH and lowered ionic strength enhance dissolution of SOM, leading
551 to the increase in DOM concentration (Evans et al., 2006). (ii) As a result of global sea level rise (Church and
552 White, 2011), freshwater wetlands are suffering seawater incursion. For example, Ardón et al. (2016) reported
553 that saltwater incursion and drought together reduced DOM export from a freshwater wetland in North Carolina
554 to the estuary by 70%. They further disentangled the combined effect of salinity and drought based on an intact
555 soil column experiment and estimated that salinity decreased DOM concentration by 29% because of stimulated
556 aggregation of DOM. This was caused by only a slight increase in salinity (up to 6 ppt), indicating a highly
557 sensitive aggregation property of DOM upon salinization. Since mangrove forests are a highly variable
558 environment in terms of salinity because of their complex hydrology (from daily change by tide to seasonal
559 change by dry vs rainy season), the aggregation–dissolution properties of SOM are highly important in
560 determining magnitude of DOM outwelling and possibly SOM accumulation rate, particularly at the mixing
561 zone. The immobilization of SOM by aggregation due to high salinity (Kida et al., 2017) and the possibility of
562 dissolution of SOM due to the decline in salinity warrant the need to investigate C dynamics in mangrove forests
563 with the aggregation–dissolution properties of SOM in mind to better understand elemental cycling in mangrove
564 forests.

565 Our data suggest that large precipitation events can strongly influence C dynamics (Fig. 3). Most
566 mangrove forests are located in tropical regions and are frequently struck by typhoons or hurricanes, which
567 causes an episodic decline in salinity. In regions with clear dry and rainy seasons, mangrove forests experience
568 a seasonal fluctuation in salinity. For example, Pérez et al. (2017) showed lower SOM and chlorophyll-a
569 contents in the subtidal sediments during the rainy season than during the dry season in a Peruvian mangrove
570 forest. They attributed this decrease in SOM to enhanced transport of SOM to the estuary because of increased
571 water flow during the rainy season. We would additionally consider a decline in river-and groundwater salinity
572 due to the increased freshwater input as an important cause of mobilization/dissolution of SOM. Similarly, in a
573 Trat mangrove forest in Eastern Thailand, groundwater salinity up to ~2 m depth throughout the entire forest is
574 completely fresh during the rainy season at least for 3 months because of increased river water flux, while
575 during the dry season the groundwater is saline (Poungparn S., pers. comm.). This seasonal change in
576 groundwater salinity could have great impacts on both SOM sequestration and DOM dynamics. Mangrove-
577 derived DOM has been suggested to be transported over long distances to coastal and offshore waters (Dittmar
578 et al., 2006, 2001). Because mangrove-derived DOM had more aromatic, light absorbing properties than coastal
579 DOM (Figs. 3, 4), exported DOM would effectively attenuate both solar UV and photosynthetically active
580 radiation, therefore directly influencing coastal primary productivity on a regional scale. Photodegradation of
581 mangrove-derived DOM in the open coastal area would also stimulate bacterial metabolism (Tranvik, 1992).
582 Overall, the contribution of the Fukido mangrove forest to the DOM concentration was estimated at
583 up to 46% of DOM and 58% of the PARAFAC components (Table 3). These results highlight the importance
584 of the mangrove forest-derived DOM (both HPO and HPI) to the coastal ocean. We proposed that the typhoon
585 event caused enhanced leaching of DOM from mangrove litter and dissolution of mangrove SOM, which was
586 otherwise retained in the mangrove soil by salinity-induced aggregation (Kida et al., 2017). The aggregation–
587 dissolution properties of SOM are crucial in determining the magnitude of DOM outwelling and expected to
588 influence SOM accumulation rate. Future studies should elucidate underlying mechanisms that control the
589 release of DOM with changing salinity, such as organo-mineral complexation. Increasing episodic freshwater
590 inputs by typhoons or hurricanes would lead to an enhanced export of mangrove-derived DOM by advective

591 exchanges of increased-DOC groundwater resulting from dissolution of SOM. Tidal hydrology and coastal
592 morphology should be important in influencing material cycling of mangrove forests as well as mangrove
593 carbon storage (Twilley et al., 2018). These characteristics affect not only biogeochemical conditions in
594 mangrove forests but also dominant mangrove species and their growth rates and microbial activity, influencing
595 SOM accumulation and turnover rates. Therefore, it is necessary to evaluate the size of the C pool and
596 outwelling of DOM and consequently the ecosystem services after classifying mangrove forests using the
597 hydrological regime as a parameter.
598
599 **Declarations of interest:** none
600
601 **Contributions:** M. K., M. Tanabe, M. Tomotsune, and N.F. collected the samples with the help of other authors.
602 M. Tanabe and M.K. conducted experiments. M. K. wrote the draft. All authors contributed to the design of the
603 study and have reviewed and approved the final article.
604
605 **Acknowledgments**
606 We are grateful to two anonymous reviewers for detailed and constructive comments on the original manuscript.
607 This study was supported by JSPS KAKENHI Grant Number JP15H05240 and Grant-in-Aid for JSPS Research
608 Fellow (17J00808).
609
610 **References**
611 Alongi, D.M., 2014. Carbon cycling and storage in mangrove forests. Ann. Rev. Mar. Sci. 6, 195–219.
612 https://doi.org/10.1146/annurev-marine-010213-135020
613 Ardón, M., Helton, A.M., Bernhardt, E.S., 2016. Drought and saltwater incursion synergistically reduce
614 dissolved organic carbon export from coastal freshwater wetlands. Biogeochemistry 127, 411–426.
615 https://doi.org/10.1007/s10533-016-0189-5
616 Benner, R., Weliky, K., Hedges, J.I., 1990. Early diagenesis of mangrove leaves in a tropical estuary:

617 Molecular-level analyses of neutral sugars and lignin-derived phenols. Geochim. Cosmochim. Acta 54,
618 1991–2001. https://doi.org/10.1016/0016-7037(90)90267-O
619 Blazevic, A., Orlowska, E., Kandioller, W., Jirsa, F., Keppler, B.K., Tafili-Kryeziu, M., Linert, W., Krachler,
620 R.F., Krachler, R., Rompel, A., 2016. Photoreduction of Terrigenous Fe-Humic Substances Leads to
621 Bioavailable Iron in Oceans. Angew. Chemie Int. Ed. 55, 6417–6422.
622 https://doi.org/10.1002/anie.201600852
623 Boehme, J.R., Coble, P.G., 2000. Characterization of colored dissolved organic matter using high-energy
624 laser fragmentation. Environ. Sci. Technol. 34, 3283–3290. https://doi.org/10.1021/es9911263
625 Bricaud, A., Morel, A., Prieur, L., 1981. Absorption by dissolved organic matter of the sea (yellow substance)
626 in the UV and visible domains. Limnol. Oceanogr. 26, 43–53. https://doi.org/10.4319/lo.1981.26.1.0043
627 Butman, D., Raymond, P.A., Butler, K., Aiken, G., 2012. Relationships between Δ 14 C and the molecular
628 quality of dissolved organic carbon in rivers draining to the coast from the conterminous United States.
629 Global Biogeochem. Cycles 26, 1–15. https://doi.org/10.1029/2012GB004361
630 Cawley, K.M., Ding, Y., Fourqurean, J., Jaffé, R., 2012. Characterising the sources and fate of dissolved
631 organic matter in Shark Bay, Australia: a preliminary study using optical properties and stable carbon
632 isotopes. Mar. Freshw. Res. 63, 1098. https://doi.org/10.1071/MF12028
633 Cawley, K.M., Yamashita, Y., Maie, N., Jaffé, R., 2014. Using optical properties to quantify fringe mangrove
634 inputs to the dissolved organic matter (DOM) pool in a subtropical estuary. Estuaries and Coasts 37,
635 399–410. https://doi.org/10.1007/s12237-013-9681-5
636 Church, J.A., White, N.J., 2011. Sea-level rise from the late 19th to the early 21st century. Surv. Geophys. 32,
637 585–602. https://doi.org/10.1007/s10712-011-9119-1
638 Dittmar, T., Hertkorn, N., Kattner, G., Lara, R.J., 2006. Mangroves, a major source of dissolved organic
639 carbon to the oceans. Global Biogeochem. Cycles 20, 7p. https://doi.org/10.1029/2005GB002570
640 Dittmar, T., Lara, R.J., 2001. Driving forces behind nutrient and organic matter dynamics in a mangrove tidal
641 creek in North Brazil. Estuar. Coast. Shelf Sci. 52, 249–259. https://doi.org/10.1006/ecss.2000.0743
642 Dittmar, T., Lara, R.J., Kattner, G., 2001. River or mangrove? Tracing major organic matter sources in

643 tropical Brazilian coastal waters. Mar. Chem. 73, 253–271. https://doi.org/10.1016/S0304-
644 4203(00)00110-9
645 Evans, C.D., Chapman, P.J., Clark, J.M., Monteith, D.T., Cresser, M.S., 2006. Alternative explanations for
646 rising dissolved organic carbon export from organic soils. Glob. Chang. Biol. 12, 2044–2053.
647 https://doi.org/10.1111/j.1365-2486.2006.01241.x
648 Fichot, G., Benner, R., 2012. The spectral slope coefficient of chromophoric dissolved organic matter (S 275
649 – 295) as a tracer of terrigenous dissolved organic carbon in river-influenced ocean margins 57, 1453–
650 1466. https://doi.org/10.4319/lo.2012.57.5.1453
651 Fox, L.E., 1983. The removal of dissolved humic acid during estuarine mixing. Estuar. Coast. Shelf Sci. 16,
652 431–440. https://doi.org/10.1016/0272-7714(83)90104-X
653 Gledhill, M., Buck, K.N., 2012. The organic complexation of iron in the marine environment: a review. Front.
654 Microbiol. 3, 1–17. https://doi.org/10.3389/fmicb.2012.00069
655 Hanley, K.W., Wollheim, W.M., Salisbury, J., Huntington, T., Aiken, G., 2013. Controls on dissolved organic
656 carbon quantity and chemical character in temperate rivers of North America. Global Biogeochem.
657 Cycles 27, 492–504. https://doi.org/10.1002/gbc.20044
658 Helms, J.R., Mao, J., Stubbins, A., Schmidt-Rohr, K., Spencer, R.G.M., Hernes, P.J., Mopper, K., 2014. Loss
659 of optical and molecular indicators of terrigenous dissolved organic matter during long-term
660 photobleaching. Aquat. Sci. 76, 353–373. https://doi.org/10.1007/s00027-014-0340-0
661 Helms, J.R., Stubbins, A., Perdue, E.M., Green, N.W., Chen, H., Mopper, K., 2013. Photochemical bleaching
662 of oceanic dissolved organic matter and its effect on absorption spectral slope and fluorescence. Mar.
663 Chem. 155, 81–91. https://doi.org/10.1016/j.marchem.2013.05.015
664 Helms, J.R., Stubbins, A., Ritchie, J.D., Minor, E.C., Kieber, D.J., Mopper, K., 2008. Absorption spectral
665 slopes and slope ratios as indicators of molecular weight, source, and photobleaching of chromophoric
666 dissolved organic matter. Limnol. Oceanogr. 53, 955–969. https://doi.org/10.4319/lo.2008.53.3.0955
667 Hu, C., Muller-Karger, F.E., Zepp, R.G., 2002. Absorbance, absorption coefficient, and apparent quantum
668 yield: A comment on common ambiguity in the use of these optical concepts. Limnol. Oceanogr. 47,

669 1261–1267. https://doi.org/10.4319/lo.2002.47.4.1261
670 Huguet, A., Vacher, L., Relexans, S., Saubusse, S., Froidefond, J.M., Parlanti, E., 2009. Properties of
671 fluorescent dissolved organic matter in the Gironde Estuary. Org. Geochem. 40, 706–719.
672 https://doi.org/10.1016/j.orggeochem.2009.03.002
673 Imai, A., Fukushima, T., Matsushige, K., Kim, Y.H., 2001. Fractionation and characterization of dissolved
674 organic matter in a shallow eutrophic lake, its inflowing rivers, and other organic matter sources. Water
675 Res. 35, 4019–4028. https://doi.org/10.1016/S0043-1354(01)00139-7
676 Kida, M., Ohtsuka, T., Kato, T., Suzuki, T., Fujitake, N., 2016. Evaluation of salinity effect on quantitative
677 analysis of aquatic humic substances using nonionic DAX-8 resin. Chemosphere 146, 129–132.
678 https://doi.org/10.1016/j.chemosphere.2015.12.031
679 Kida, M., Tomotsune, M., Iimura, Y., Kinjo, K., Ohtsuka, T., Fujitake, N., 2017. High salinity leads to
680 accumulation of soil organic carbon in mangrove soil. Chemosphere 177, 51–55.
681 https://doi.org/10.1016/j.chemosphere.2017.02.074
682 Kothawala, D.N., Murphy, K.R., Stedmon, C.A., Weyhenmeyer, G.A., Tranvik, L.J., 2013. Inner filter
683 correction of dissolved organic matter fluorescence. Limnol. Oceanogr. Methods 11, 616–630.
684 https://doi.org/10.4319/lom.2013.11.616
685 Kristensen, E., Bouillon, S., Dittmar, T., Marchand, C., 2008. Organic carbon dynamics in mangrove
686 ecosystems: A review. Aquat. Bot. 89, 201–219. https://doi.org/10.1016/j.aquabot.2007.12.005
687 Lee, S.Y., 1995. Mangrove outwelling: a review. Hydrobiologia 295, 203–212.
688 https://doi.org/10.1007/BF00029127
689 Maher, D.T., Santos, I.R., Golsby-Smith, L., Gleeson, J., Eyre, B.D., 2013. Groundwater-derived dissolved
690 inorganic and organic carbon exports from a mangrove tidal creek: The missing mangrove carbon sink?
691 Limnol. Oceanogr. 58, 475–488. https://doi.org/10.4319/lo.2013.58.2.0475
692 Maie, N., Parish, K.J., Watanabe, A., Knicker, H., Benner, R., Abe, T., Kaiser, K., Jaffé, R., 2006. Chemical
693 characteristics of dissolved organic nitrogen in an oligotrophic subtropical coastal ecosystem. Geochim.
694 Cosmochim. Acta 70, 4491–4506. https://doi.org/10.1016/j.gca.2006.06.1554

695 Maie, N., Pisani, O., Jaffé, R., 2008. Mangrove tannins in aquatic ecosystems: Their fate and possible
696 influence on dissolved organic carbon and nitrogen cycling. Limnol. Oceanogr. 53, 160–171.
697 Maie, N., Scully, N.M., Pisani, O., Jaffé, R., 2007. Composition of a protein-like fluorophore of dissolved
698 organic matter in coastal wetland and estuarine ecosystems. Water Res. 41, 563–570.
699 https://doi.org/10.1016/j.watres.2006.11.006
700 Maie, N., Sekiguchi, S., Watanabe, A., Tsutsuki, K., Yamashita, Y., Melling, L., Cawley, K.M., Shima, E.,
701 Jaffé, R., 2014. Dissolved organic matter dynamics in the oligo/meso-haline zone of wetland-influenced
702 coastal rivers. J. Sea Res. 91, 58–69. https://doi.org/10.1016/j.seares.2014.02.016
703 Maie, N., Yamashita, Y., Cory, R.M., Boyer, J.N., Jaffé, R., 2012. Application of excitation emission matrix
704 fluorescence monitoring in the assessment of spatial and seasonal drivers of dissolved organic matter
705 composition: Sources and physical disturbance controls. Appl. Geochemistry 27, 917–929.
706 https://doi.org/10.1016/j.apgeochem.2011.12.021
707 Maie, N., Yang, C., Parish, K., Jaffe, R., 2005. Chemical characteristics of dissolved organic matter in an
708 oligotrophic subtropical wetland / estuarine ecosystem 50, 23–35.
709 McKnight, D.M., Boyer, E.W., Westerhoff, P.K., Doran, P.T., Kulbe, T., Andersen, D.T., 2001.
710 Spectrofluorometric characterization of dissolved organic matter for indication of precursor organic
711 material and aromaticity. Limnol. Oceanogr. 46, 38–48. https://doi.org/10.4319/lo.2001.46.1.0038
712 Murphy, K.R., 2011. A note on determining the extent of the water Raman peak in fluorescence spectroscopy.
713 Appl. Spectrosc. 65, 233–236. https://doi.org/10.1366/10-06136
714 Murphy, K.R., Hambly, A., Singh, S., Henderson, R.K., Baker, A., Stuetz, R., Khan, S.J., 2011. Organic
715 matter fluorescence in municipal water recycling schemes: Toward a unified PARAFAC model.
716 Environ. Sci. Technol. 45, 2909–2916. https://doi.org/10.1021/es103015e
717 Murphy, K.R., Stedmon, C.A., Graeber, D., Bro, R., 2013. Fluorescence spectroscopy and multi-way
718 techniques. PARAFAC. Anal. Methods 5, 6557–6566. https://doi.org/10.1039/c3ay41160e
719 Murphy, K.R., Stedmon, C.A., Wenig, P., Bro, R., 2014. OpenFluor- an online spectral library of auto-
720 fluorescence by organic compounds in the environment. Anal. Methods 6, 658–661.

https://doi.org/10.1039/c3ay41935e

Murphy, K.R., Timko, S.A., Gonsior, M., Powers, L.C., Wünsch, U.J., Stedmon, C.A., 2018. Photochemistry illuminates ubiquitous organic matter fluorescence spectra. Environ. Sci. Technol. 52, 11243–11250. https://doi.org/10.1021/acs.est.8b02648

Odum, W.E., 1968. A research challenge: evaluating the productivity of coastal and estuarine water. Proc. Second Sea Grant Conf. 63–64.

Ohtsuka, T., Tomotsune, M., Suchewaboripont, V., Iimura, Y., Kida, M., Yoshitake, S., Kondo, M., Kinjo, K., 2019. Stand dynamics and aboveground net primary productivity of a mature subtropical mangrove forest on Ishigaki Island, south-western Japan. Reg. Stud. Mar. Sci. 100516. https://doi.org/10.1016/j.rsma.2019.100516

Osburn, C.L., Boyd, T.J., Montgomery, M.T., Bianchi, T.S., Coffin, R.B., Paerl, H.W., 2016. Optical proxies for terrestrial dissolved organic matter in estuaries and coastal waters. Front. Mar. Sci. 2. https://doi.org/10.3389/fmars.2015.00127

Pérez, A., Gutiérrez, D., Saldarriaga, M.S., Sanders, C.J., 2017. Hydrological controls on the biogeochemical dynamics in a Peruvian mangrove forest. Hydrobiologia 803, 69–86. https://doi.org/10.1007/s10750-017-3118-2

Ray, R., Baum, A., Rixen, T., Gleixner, G., Jana, T.K., 2018. Exportation of dissolved (inorganic and organic) and particulate carbon from mangroves and its implication to the carbon budget in the Indian Sundarbans. Sci. Total Environ. 621, 535–547. https://doi.org/10.1016/j.scitotenv.2017.11.225

Santín, C., Yamashita, Y., Otero, X.L., Álvarez, M.Á., Jaffé, R., 2009. Characterizing humic substances from estuarine soils and sediments by excitation-emission matrix spectroscopy and parallel factor analysis. Biogeochemistry 96, 131–147. https://doi.org/10.1007/s10533-009-9349-1

Santos, I.R., Eyre, B.D., Huettel, M., 2012. The driving forces of porewater and groundwater flow in permeable coastal sediments: A review. Estuar. Coast. Shelf Sci. 98, 1–15. https://doi.org/10.1016/j.ecss.2011.10.024

Sholkovitz, E.R., 1976. Flocculation of dissolved organic and inorganic matter during the mixing of river

747 water and seawater. Geochim. Cosmochim. Acta 40, 831–845. https://doi.org/10.1016/0016-
748 7037(76)90035-1
749 Soto Cárdenas, C., Gerea, M., Garcia, P.E., Pérez, G.L., Diéguez, M.C., Rapacioli, R., Reissig, M.,
750 Queimaliños, C., 2017. Interplay between climate and hydrogeomorphic features and their effect on the
751 seasonal variation of dissolved organic matter in shallow temperate lakes of the Southern Andes
752 (Patagonia, Argentina): a field study based on optical properties. Ecohydrology 10, e1872.
753 https://doi.org/10.1002/eco.1872
754 Spencer, R.G., Butler, K.D., Aiken, G.R., 2012. Dissolved organic carbon and chromophoric dissolved
755 organic matter properties of rivers in the USA. J. Geophys. Res. 117, 1–14.
756 https://doi.org/10.1029/2011JG001928
757 Spencer, R.G.M., Aiken, G.R., Wickland, K.P., Striegl, R.G., Hernes, P.J., 2008. Seasonal and spatial
758 variability in dissolved organic matter quantity and composition from the Yukon River basin, Alaska.
759 Global Biogeochem. Cycles 22, 1–13. https://doi.org/10.1029/2008GB003231
760 Stedmon, C., Markager, S., 2005a. Resolving the variability in dissolved organic matter fluorescence in a
761 temperate estuary and its catchment using PARAFAC analysis. Limnol. Oceanogr. 50, 686–697.
762 https://doi.org/10.4319/lo.2005.50.2.0686
763 Stedmon, C., Markager, S., 2005b. Tracing the production and degradation of autochthonous fractions of
764 dissolved organic matter by fluorescence analysis. Limnol. Oceanogr. 50, 1415–1426.
765 https://doi.org/10.4319/lo.2005.50.5.1415
766 Stieglitz, T.C., Clark, J.F., Hancock, G.J., 2013. The mangrove pump: The tidal flushing of animal burrows in
767 a tropical mangrove forest determined from radionuclide budgets. Geochim. Cosmochim. Acta 102, 12–
768 22. https://doi.org/10.1016/j.gca.2012.10.033
769 Thurman, E.M., Malcolm, R.L., 1981. Preparative isolation of aquatic humic substances. Environ. Sci.
770 Technol. 15, 463–466. https://doi.org/10.1021/es00086a012
771 Tranvik, L.J., 1992. Allochthonous dissolved organic matter as an energy source for pelagic bacteria and the
772 concept of the microbial loop. Hydrobiologia 229, 107–114. https://doi.org/10.1007/BF00006994

773 Tsuda, K., Takata, A., Shirai, H., Kozaki, K., Fujitake, N., 2012. A method for quantitative analysis of aquatic
774 humic substances in clear water based on carbon concentration. Anal. Sci. 28, 1017–1020.
775 https://doi.org/10.2116/analsci.28.1017
776 Twilley, R., 1985. The exchange of organic carbon in basin mangrove forests in a southwest Florida estuary.
777 Estuar. Coast. Shelf Sci. 20, 543–557.
778 Twilley, R.R., Rovai, A.S., Riul, P., 2018. Coastal morphology explains global blue carbon distributions.
779 Front. Ecol. Environ. 1–6. https://doi.org/10.1002/fee.1937
780 Wafar, S., Untawale, A.G., Wafar, M., 1997. Litter fall and energy flux in a mangrove ecosystem. Estuar.
781 Coast. Shelf Sci. 44, 111–124. https://doi.org/10.1006/ecss.1996.0152
782 Weishaar, J.L., Aiken, G.R., Bergamaschi, B.A., Fram, M.S., Fujii, R., Mopper, K., 2003. Evaluation of
783 specific ultraviolet absorbance as an indicator of the chemical composition and reactivity of dissolved
784 organic carbon. Environ. Sci. Technol. 37, 4702–4708. https://doi.org/10.1021/es030360x
785 Yamashita, Y., Fichot, C.G., Shen, Y., Jaffé, R., Benner, R., 2015. Linkages among fluorescent dissolved
786 organic matter, dissolved amino acids and lignin-derived phenols in a river-influenced ocean margin.
787 Front. Mar. Sci. 2, 1–14. https://doi.org/10.3389/fmars.2015.00092
788 Yamashita, Y., Scinto, L.J., Maie, N., Jaffé, R., 2010. Dissolved organic matter characteristics across a
789 subtropical wetland's landscape: Application of optical properties in the assessment of environmental
790 dynamics. Ecosystems 13, 1006–1019. https://doi.org/10.1007/s10021-010-9370-1
791

Table 1. Sampling dates, basic water chemistry, DOM concentration and composition, and its optical data

yyyy/mm/dd	Salinity	pH	DOM	%HPO	$SUVA_{254}$	$S_{275–295}$	BIX	yyyy/mm/dd	Salinity	pH	DOM	%HPO	$SUVA_{254}$	$S_{275–295}$	BIX
			mg C L^{-1}		L mg C^{-1} m^{-1}	nm^{-1}					mg C L^{-1}		L mg C^{-1} m^{-1}	nm^{-1}	
2014/9/30	0.2	7.4	0.90	68.8	4.1	0.013	ND	2015/8/25	0.2	7.8	1.61	69.6	3.3	0.013	0.60
	0.4	7.4	1.26	66.0	4.2	0.012	ND		1.6	8.2	3.21	63.1	3.4	0.015	0.68
	11.3	7.3	1.60	64.3	3.8	0.014	ND		2.4	8.1	2.29	63.4	3.4	0.013	0.66
	24.7	7.3	1.67	61.1	3.3	0.016	ND		4.0	8.1	2.32	61.3	3.4	0.014	0.62
	29.8	7.4	1.39	57.7	3.1	0.017	ND		6.1	8.0	2.11	57.6	3.2	0.014	0.69
	32.2	8.0	0.67	50.5	2.1	0.019	ND		11.4	8.0	2.07	58.9	3.0	0.014	0.66
									25.7	8.1	1.29	39.0	2.0	0.016	0.83
2014/11/21	0.2	7.3	0.99	64.8	3.6	0.012	ND	2015/8/26	0.2	8.0	1.63	68.2	3.0	-	0.68
	6.7	7.7	1.33	57.9	3.4	0.016	ND		1.0	8.3	3.71	63.1	3.8	-	0.66
	14.3	7.6	1.56	60.0	3.5	0.016	ND		1.5	8.2	2.55	65.0	3.5	-	0.72
	22.4	7.5	1.55	57.7	3.3	0.017	ND		1.8	8.2	2.42	60.5	3.3	-	0.69
	27.9	7.6	1.29	52.5	2.7	0.018	ND		2.4	8.1	2.58	64.9	3.4	-	0.68
	30.9	7.8	0.93	52.6	2.5	0.017	ND		3.1	8.0	2.38	63.2	3.3	-	0.66
									10.0	8.2	2.03	57.3	2.7	-	0.71
2015/1/23	0.2	7.2	0.86	67.9	ND	ND	ND	2015/11/10	0.2	7.2	1.00	66.6	4.1	0.012	0.67
	4.2	7.4	1.16	60.4	ND	ND	ND		10.0	7.2	2.10	62.8	3.7	0.016	0.61
	8.5	7.4	1.22	62.2	ND	ND	ND		10.4	7.4	1.63	59.1	3.6	0.015	0.61
	17.1	7.4	1.32	58.4	ND	ND	ND		17.1	7.4	1.55	55.4	3.6	0.015	0.73
	23.8	7.4	1.12	53.5	ND	ND	ND		18.0	7.4	1.32	58.6	3.3	0.015	0.68
	28.4	7.5	1.12	47.5	ND	ND	ND		26.2	7.6	1.12	54.1	3.0	0.016	0.76
	32.7	7.8	1.10	45.9	ND	ND	ND		32.7	8.2	0.79	42.3	2.1	0.012	-
2015/5/14	0.1	7.7	1.07	65.0	4.2	0.012	ND	2016/3/8	0.3	7.6	0.91	68.5	3.8	0.013	0.61
	3.0	7.8	1.54	63.6	3.8	0.013	ND		0.4	7.5	1.11	66.0	3.5	0.013	0.67
	3.8	7.8	1.54	64.3	3.8	0.013	ND		2.7	7.6	1.18	67.3	3.9	0.013	0.57
	8.2	7.9	1.64	55.8	3.8	0.014	ND		5.4	7.5	1.18	67.3	3.6	0.014	0.57
	12.9	7.7	1.34	52.2	3.8	0.015	ND		10.0	7.4	1.17	61.8	3.2	0.015	0.61
	18.7	7.8	1.32	57.1	3.3	0.015	ND		17.9	7.5	1.22	59.2	2.9	0.015	0.62
	20.2	7.9	1.21	57.7	3.0	0.014	ND		29.8	8.0	0.98	45.5	1.5	0.018	0.83
2015/8/24	0.3	7.1	1.55	71.0	3.1	-	0.55	2016/6/20	0.1	7.3	1.78	68.2	4.1	0.011	0.64
	1.7	7.6	3.20	63.0	3.6	-	0.61		0.4	7.5	0.77	56.1	3.1	0.012	0.66
	1.7	7.5	2.11	62.9	3.3	-	0.58		3.3	7.5	1.56	65.6	3.8	0.012	0.57
	3.6	7.7	2.12	60.3	3.2	-	0.62		10.6	7.4	1.56	59.8	3.5	0.014	0.57
	5.9	7.7	2.02	57.4	3.1	-	0.74		16.7	7.4	1.47	59.1	3.3	0.014	0.60
	8.4	7.9	1.90	59.8	3.0	-	0.69		23.7	7.4	1.17	54.6	3.0	0.014	0.61
	32.2	8.2	0.88	33.6	0.8	-	0.93		31.2	7.9	1.03	43.1	1.7	0.016	0.78

ND not determined

$S_{275–295}$ on 24 and 26 August 2015 was not used due to disturbance of spectra caused by auto-switching of the light source of the spectrophotometer during measurements.

DOM= dissolved organic matter, %HPO = proportion of hydrophobic fraction in DOM, $SUVA_{254}$ = specific UV absorbance at 254 nm, $S_{275–295}$ = spectral slope determined between 275 nm and 295 nm, and BIX = biological index.

Table 2. Characteristics of the three PARAFAC components derived from the Fukido River.

Component	Excitation Maximum	Emission maximum	Origin	Assignment	Reference
C_{480}	< 265 (360)	478	Terrestrial/ autochthonous	highly conjugated aromatic material resemble isolated fulvic acids from soils and sediments	Osburn et al., 2016
				ubiquitous humic-like	Stedmon and Markager., 2005a Yamashita et al., 2010
C_{410}	< 265 (325)	409	Terrestrial/ autochthonous/ anthropogenic	ubiquitous humic-like suggested as photo-labile and agricultural land use derived	Stedmon and Markager., 2005a Yamashita et al., 2010
				fulvic acid-type, suggested to be bio-available	Cawley et al., 2012
C_{380}	< 265 (275)	380	Terrestrial/ autochthonous	combination of protein-like component and UV-C humic component	
				photo-refractory or photo-producible	Murphy et al., 2018

Table 3. Contribution of the mangrove forest to DOM fractions and PARAFAC components (in percentage).

Sampling date	DOM	HPO	HPI	C_{480}	C_{410}	C_{380}
30-Sep-14	46.2	47.6*	44.1	ND	ND	ND
21-Nov-14	28.8	27.8	30.2	ND	ND	ND
23-Jan-15	16.6*	17.9	15.0*	ND	ND	ND
14-May-15	18.9	13.7	25.2*	ND	ND	ND
24-Aug-15§	20.5	16.8*	25.8	40.4	43.8	58.1
25-Aug-15§	27.1	21.5*	33.0	41.5	49.1	42.6
26-Aug-15§	24.2	22.2*	27.3	29.0	33.6	31.9
10-Nov-15	31.3	34.2	27.8	43.4	47.0	18.7*
8-Mar-16	17.2	20.7	12.1*	36.9	40.6	−19.4*
20-Jun-16	30.3	39.7	17.1*	47.0	49.2	20.9

* not significantly different from the conservative mixing (F-test, $P > 0.05$).

§ typhoon event (see the main text)

Figure 1. a) Fukido mangrove forest on Ishigaki Island, Okinawa, Japan. The white solid line indicates the mangrove forest area. The dotted line indicates the Fukido River from which water samples were collected. Black dots with white circles indicate the surface water sampling points, while the black square with white frame indicates groundwater sampling point. On every sampling day, salinity continuously increased from the headwater to the sea sampling point. b) monthly average precipitation and air temperature record between 1981 and 2010.

Figure 2. Daily precipitation record and sampling timing. Arrows indicate the sampling timing with B denoting baseflow condition (any period more than 24 h after a rain event). On 24–26 August 2015, successive three-day sampling was conducted to capture the changes in dissolved organic matter concentrations and compositions caused by heavy rains due to Typhoon Goni. The precipitation on 23, 24, 25 and 26 August 2015 was 241, 33, 54 and 14 mm, respectively.

Figure 3. Dissolved organic matter (DOM) and hydrophobic and hydrophilic fraction of DOM (HPO and HPI) concentrations (upper row), F_{max} of the identified PARAFAC components (middle row), and the relative distribution of the PARAFAC components (bottom row), all plotted along salinity. The left panel shows the results under baseflow condition, while the right panel is the results during the typhoon event. Solid lines are an example of simple conservative mixing model lines connecting headwater and the sea for 20 June 2016 samples (left panel) and 24 August 2015 samples (right panel). Note the different scale of the y-axis between the left and right panels.

Figure 4. (a) proportion of hydrophobic fraction in DOM (%HPO), (b) specific UV absorbance at 254 nm ($SUVA_{254}$), (c) biological index (BIX), and (d) spectral slope determined between 275 nm and 295 nm ($S_{275–295}$) along the salinity gradient. White circles represent samples collected under the baseflow conditions, while black circles indicate samples during the typhoon event.

Figure 5. Groundwater DOC concentration at different depth collected every 2 h for 24 h on 8 March 2016. The regression line (least squares) is indicated by a solid line, where the x-intercept is 1.27 mg C L^{-1}. The first collected samples (represented by white circle) were omitted from the regression analysis due to contamination possibly from the vinyl chloride pipe and plastic syringe used for groundwater collection.

Figure 1

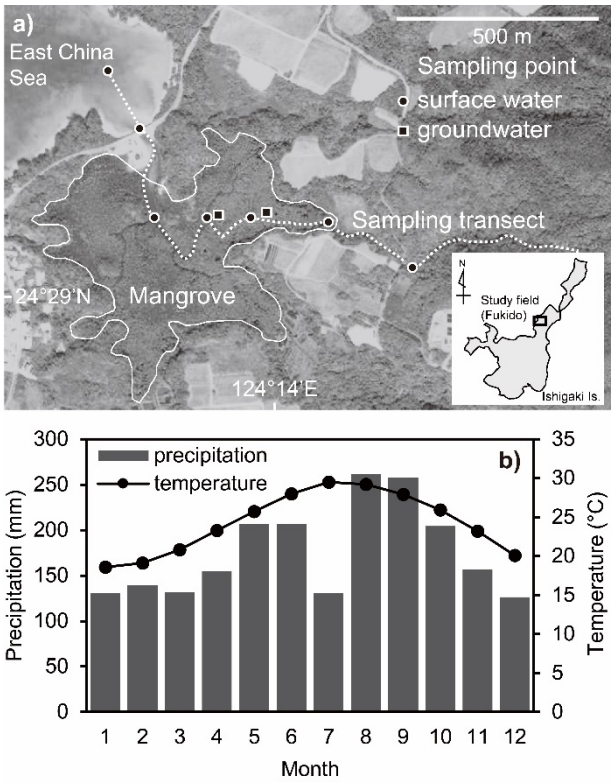

Figure 2

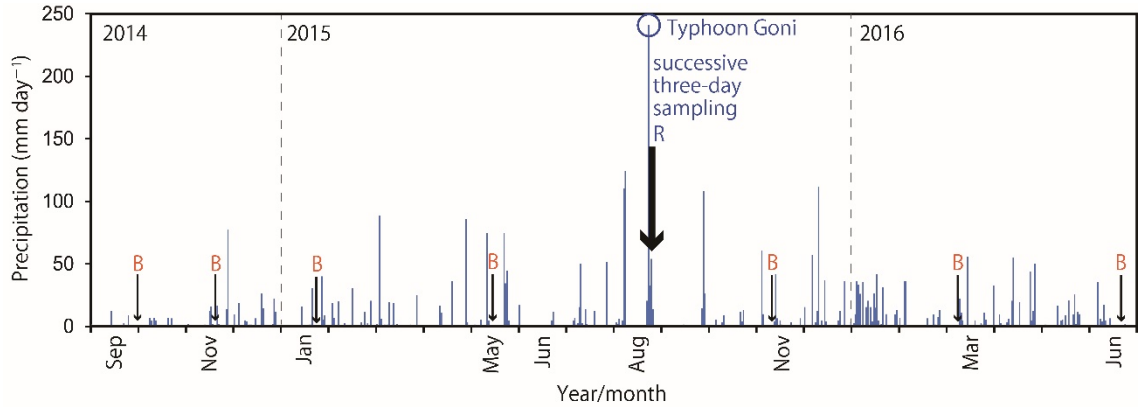

Figure 3

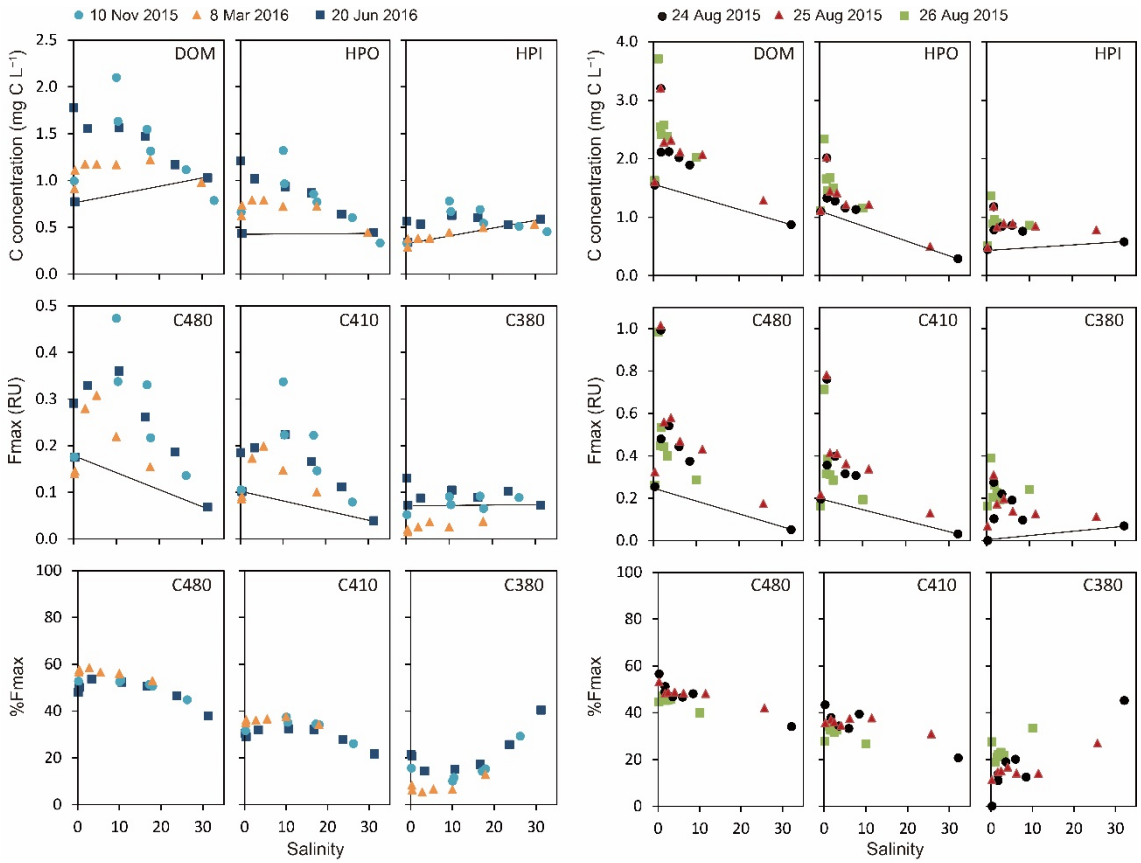
10 Nov 2015
8 Mar 2016
20 Jun 2016
24 Aug 2015
25 Aug 2015
26 Aug 2015
DOM
HPO
HPI
C480
C410
C380
C concentration (mg C L⁻¹)
Fmax (RU)
%Fmax
Salinity

Figure 4

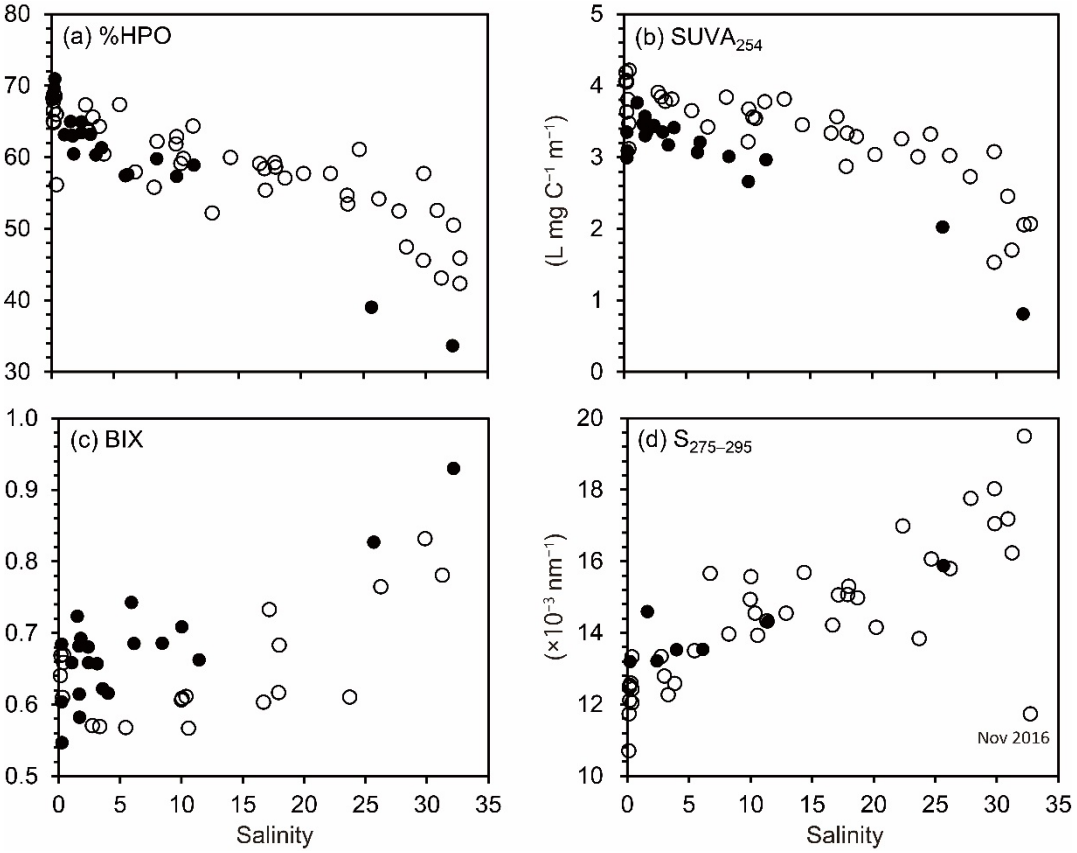

Figure 5

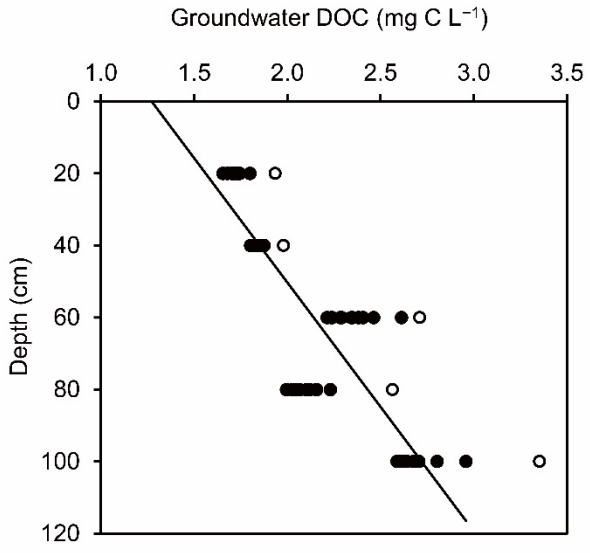

Supporting information for:

Changes in dissolved organic matter composition and dynamics in a subtropical mangrove river driven by rainfall

Journal: Estuarine, Coastal and Shelf Science

Morimaru Kida[1†‡*], Mai Tanabe[1], Mitsutoshi Tomotsune[1¶], Shinpei Yoshitake[2] Kazutoshi Kinjo[3], Toshiyuki Ohtsuka[4], and Nobuhide Fujitake[1]

1 Graduate School of Agricultural Science, Kobe University, 1 Rokkodai, Nada, Kobe, Hyogo 657-8501, Japan

†Research Fellow of Japan Society for the Promotion of Science

2 Takayama Field Station, River Basin Research Center, Gifu University, 919-47, Iwai, Takayama, Gifu 506-0815, Japan

3 Faculty of Agriculture, University of the Ryukyus, 1 Senbaru, Nishihara, Nakagami, Okinawa 903-0213, Japan

4 River Basin Research Center, Gifu University, 1-1 Yanagito, Gifu, Gifu 501-1193, Japan

‡ Present address: Research Group for Marine Geochemistry (ICBM-MPI Bridging Group), Carl von Ossietzky University of Oldenburg, Institute for Chemistry and Biology of the Marine Environment (ICBM), Carl-von-Ossietzky-Str. 9-11, 26129 Oldenburg, Germany

¶ Present address: Faculty of Education and Integrated Arts and Sciences, Waseda University, 2-2 Wakamatsu, Shinjuku, Tokyo 162–8480, Japan

*Corresponding author: Morimaru Kida

Address: marumori1004@gmail.com

Tell: 078-803-5846

ORCID ID: 0000-0002-9908-2012 (M.K.)

Content: 4 figures & 1 table

Table S1. Data of a preliminary sampling on 14 May 2013 when a heavy rain (57 mm) was observed one day before sampling.

Salinity	pH	DOM	HPO	HPI	%HPO
		(mg C L^{-1})	(mg C L^{-1})	(mg C L^{-1})	
0.1	7.4	1.41	1.07	0.34	75.9
0.5	7.5	1.48	1.05	0.42	71.5
1.8	7.6	1.48	1.01	0.47	68.5
3.2	7.6	1.46	0.96	0.50	65.5
5.3	7.6	1.52	0.95	0.56	63.0
8.9	7.6	1.22	0.75	0.48	61.1
27.7	8.1	0.92	0.44	0.49	47.5

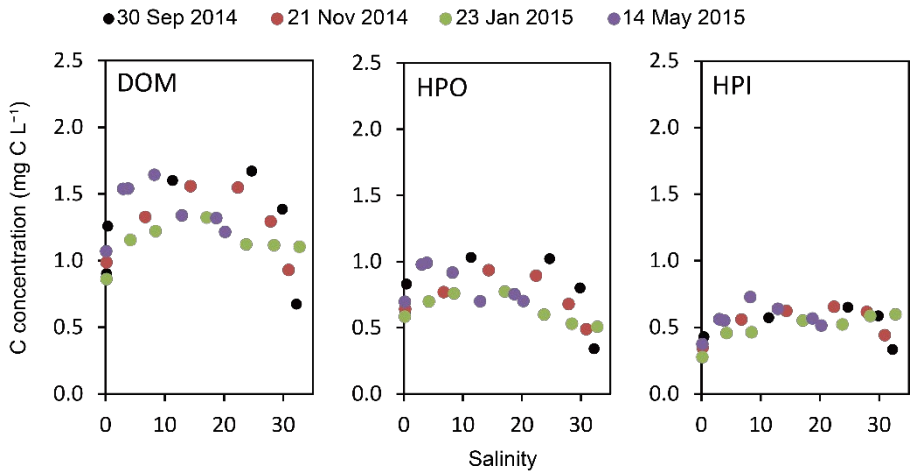

Figure S1. Dissolved organic matter (DOM) and hydrophobic and hydrophilic fraction of DOM (HPO and HPI) concentrations plotted along salinity.

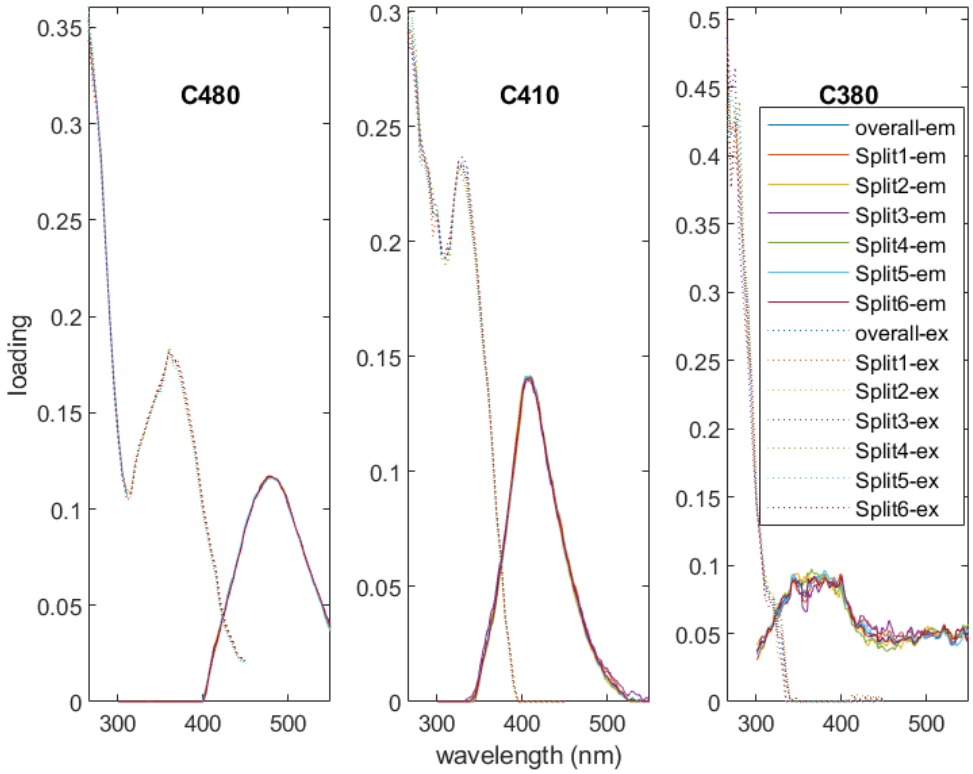

Figure S2. Loadings of excitation and emission spectra of the identified PARAFAC components (*overall-ex* and *overall-em*) and the result of split-half analysis (*Split1–6*). The dotted and solid curves represent excitation and emission spectra, respectively.

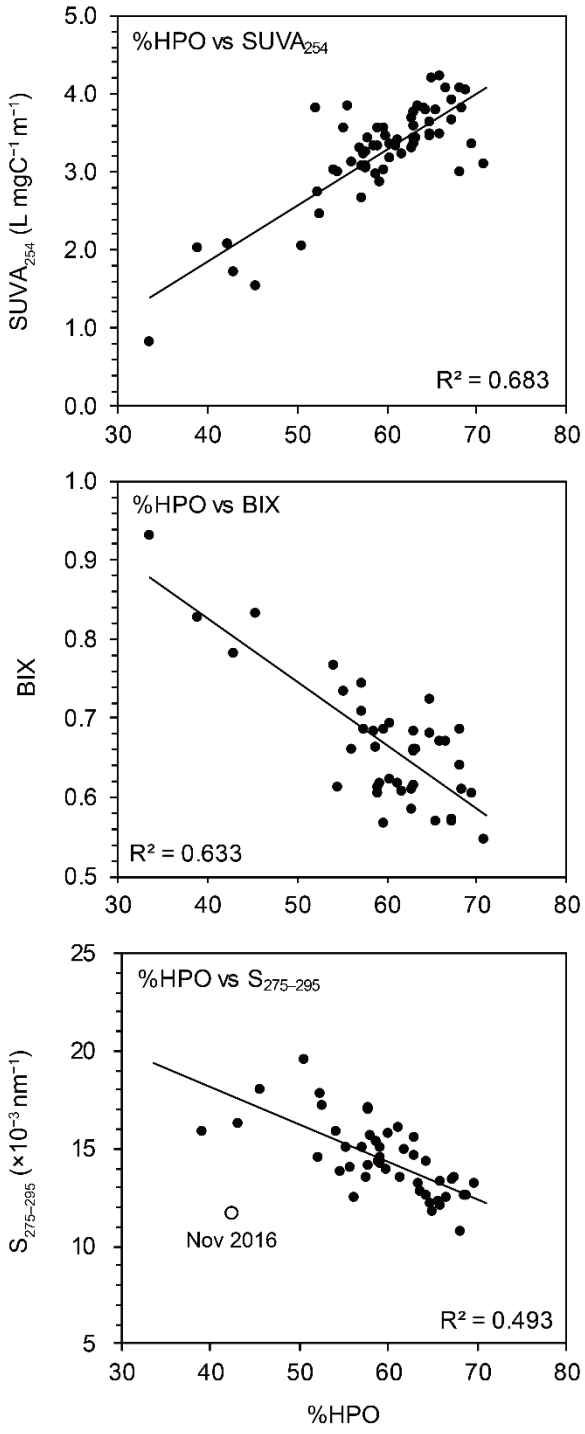

Figure S3. Relationships between the amount of hydrophobic fraction of DOM (%HPO, on carbon basis) and specific ultraviolet absorbance ($SUVA_{254}$), biological index (BIX), and spectral slope determined between 275 nm and 295 nm ($S_{275–295}$) for the Fukido River. The relationship between %HPO and $S_{275–295}$ was analyzed excluding an outlier (seawater sample collected in November 2016, represented by a white circle).

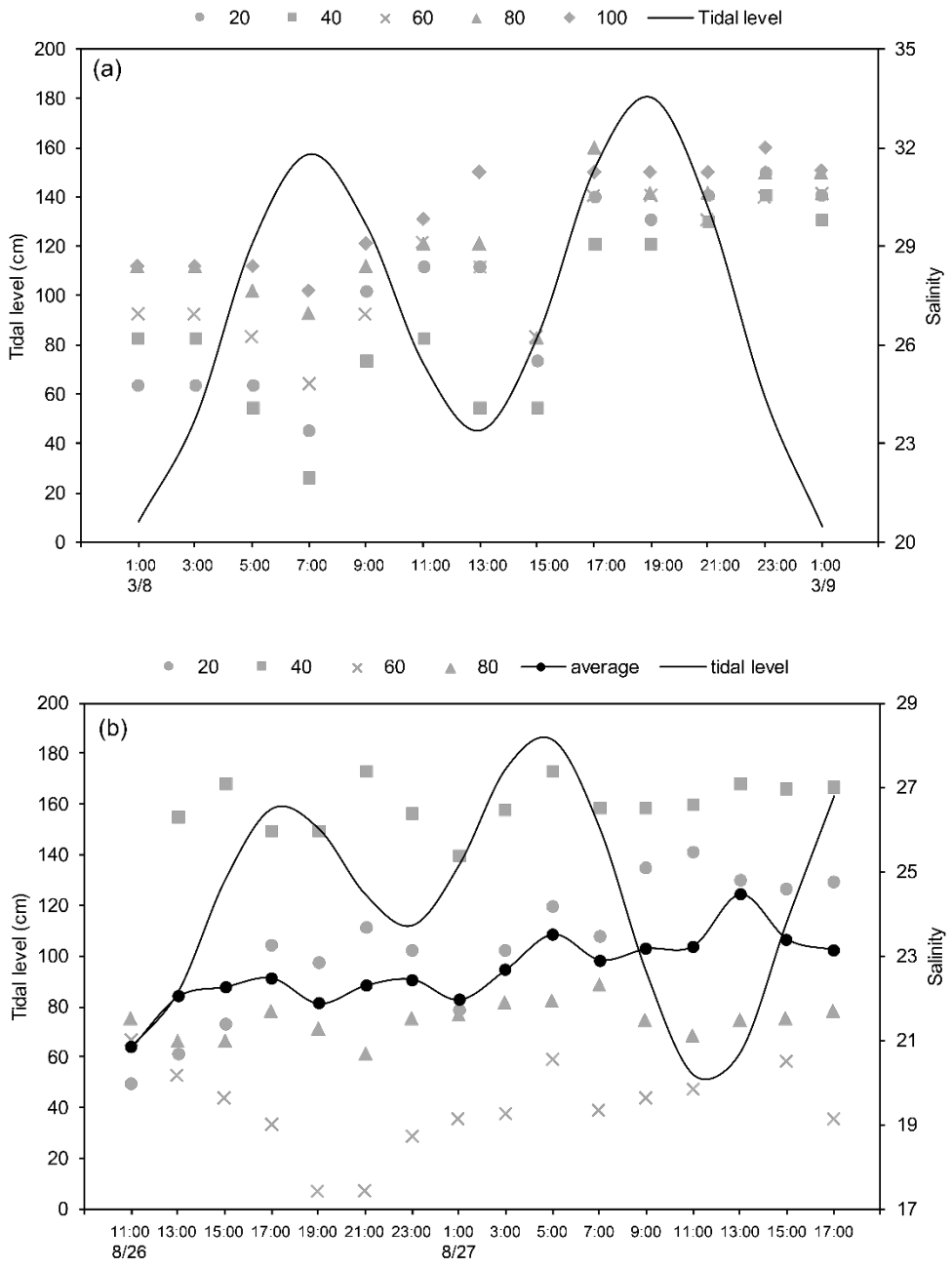

Figure S4. Groundwater salinity on (a) 8 March 2016 under the baseflow condition and (b) 26–27 August 2015 three days after Typhoon Goni. Average salinity values are presented for 26–27 August 2015 sampling to make the salinity trend clear. Black solid line represents the tidal level. Note the difference in y-scale for salinity.